AeroChem TP-349

BORON COMBUSTION PRODUCT CHEMISTRY

WILLIAM J. MILLER
AEROCHEM RESEARCH LABORATORIES, INC.
P.O. BOX 12
PRINCETON, NEW JERSEY 08540

October 1976
Final Report for Period 1 March 1974 - 31 August 1976

Prepared for
OFFICE OF NAVAL RESEARCH
DEPARTMENT OF THE NAVY
ARLINGTON, VA 22217

AeroChem TP-349

BORON COMBUSTION PRODUCT CHEMISTRY

WILLIAM J. MILLER
AEROCHEM RESEARCH LABORATORIES, INC.
P.O. BOX 12
PRINCETON, NEW JERSEY 08540

October 1976
Final Report for Period 1 March 1974 - 31 August 1976

Prepared for
OFFICE OF NAVAL RESEARCH
DEPARTMENT OF THE NAVY
ARLINGTON, VA 22217

This research was sponsored by the Office of Naval Research, Contract No. N00014-74-C-0326, ONR Contract Authority No. NR 092-547/1-4-74 (473).

UNCLASSIFIED

SECURITY CLASSIFICATION OF THIS PAGE (When Data Entered)

REPORT DOCUMENTATION PAGE

READ INSTRUCTIONS BEFORE COMPLETING FORM

1. REPORT NUMBER	2. GOVT ACCESSION NO. / 3. RECIPIENT'S CATALOG NUMBER
4. TITLE (and Subtitle): BORON COMBUSTION PRODUCT CHEMISTRY	5. TYPE OF REPORT & PERIOD COVERED: FINAL REPORT, 1 Mar [illegible] 974 – 31 Aug [illegible] 976
	6. PERFORMING ORG. REPORT NUMBER: TP-349
7. AUTHOR(s): William J. Miller	8. CONTRACT OR GRANT NUMBER(s): N00014-74-C-0326
9. PERFORMING ORGANIZATION NAME AND ADDRESS: AeroChem Research Laboratories, Inc. P.O. Box 12 Princeton, NJ 08540	10. PROGRAM ELEMENT, PROJECT, TASK AREA & WORK UNIT NUMBERS: 12 125 p.
11. CONTROLLING OFFICE NAME AND ADDRESS: Office of Naval Research Department of the Navy Arlington, VA 22217	12. REPORT DATE: Oct [illegible] 1976
	13. NUMBER OF PAGES: 69
14. MONITORING AGENCY NAME & ADDRESS (if different from Controlling Office)	15. SECURITY CLASS. (of this report): Unclassified
	15a. DECLASSIFICATION/DOWNGRADING SCHEDULE

16. DISTRIBUTION STATEMENT (of this Report)

Approved for public release; Distribution unlimited

17. DISTRIBUTION STATEMENT (of the abstract entered in Block 20, if different from Report)

18. SUPPLEMENTARY NOTES

19. KEY WORDS (Continue on reverse side if necessary and identify by block number)

Nucleation
Boron Oxides
Boric Acids
Combustion
Supersonic Jets

20. ABSTRACT (Continue on reverse side if necessary and identify by block number)

This study comprises an experimental investigation of the chemistry of boron combustion products with particular emphasis on the phenomena preceding and accompanying nucleation in expanding flows. Supersonic (Mach number $\gtrsim 3$) jets of the burnt gases from $H_2/O_2/N_2$ flames seeded with BCl_3 were examined using laser light scattering and a mass spectrometer equipped with a modulated molecular beam sampling system. The results demonstrate that the processes by which the primary combustion product HBO_2 is converted to condensed phase jet constituents such as B_2O_3(liquid) are not interpretable via models based

DD FORM 1 JAN 73 1473 EDITION OF 1 NOV 65 IS OBSOLETE

UNCLASSIFIED

SECURITY CLASSIFICATION OF THIS PAGE (When Data Entered)

(Block 20, continued)

on conventional homogeneous nucleation theories. The dehydration corresponding to the overall process $2HBO_2 \rightarrow B_2O_3(liquid) + H_2O$ is found not to occur at any discreet step in the reaction scheme but rather appears to occur gradually. Rate coefficients for the reactions $2HBO_2 \rightarrow (HBO_2)_2$ and $HBO_2 + (HBO_2)_2 \rightarrow (HBO_2)_3$ have been determined at a temperature of 650 K to be 8×10^{-11} and 3×10^{-10} ml molecule^{-1} sec^{-1}, respectively. Additional experiments on dissociative electron attachment to HBO_2 and HCl have produced a rate coefficient of 3.2×10^{-10} exp(-11,000/T) ml molecule^{-1} sec^{-1} for the reaction $e^- + HBO_2 \rightarrow BO_2^- + H$ and a value of 6×10^{-11} exp(-10,100/T) ml molecule^{-1} sec^{-1} for $e^- + HCl \rightarrow Cl^- + H$.

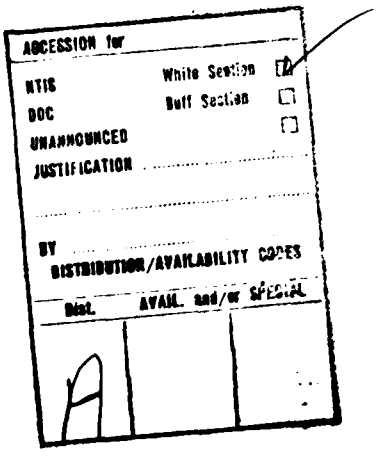

SUMMARY

This study comprises an experimental investigation of the chemistry of boron combustion products with particular emphasis on the phenomena preceding and accompanying nucleation in expanding flows. Supersonic (Mach number $\gtrsim 3$) jets of the burnt gases from $H_2/O_2/N_2$ flames seeded with BCl_3 were examined using laser light scattering and a mass spectrometer equipped with a modulated molecular beam sampling system. The results demonstrate that the processes by which the primary combustion product HBO_2 is converted to condensed phase jet constituents such as B_2O_3(liquid) are not interpretable via models based on conventional homogeneous nucleation theories. Mass spectrometric probing of systems held close to conditions favoring particle formation reveal that the reaction mechanisms are extremely complex and involve a wide variety of intermediate species of widely varying H/B/O proportions. The dehydration corresponding to the overall process $2HBO_2 \rightarrow B_2O_3$(liquid) + H_2O is found not to occur at any discreet step in the reaction scheme, but rather appears to occur gradually and is still proceeding even when the bulk of the boron present is in the form of species with molecular weights between 150 and 500 amu. The mechanistic path to molecules with molecular weights in excess of 135 seems to proceed through addition of the 'monomers' HBO_2, B_2O_3 and, less often, H_3BO_3 to a series of substrates of which $H_2B_3O_5$ is the lowest member.

Rate coefficients for the reactions leading to the dimer and trimer of HBO_2, viz.,

$$2HBO_2 \rightarrow (HBO_2)_2 \text{ and } HBO_2 + (HBO_2)_2 \rightarrow (HBO_2)_3$$

have been determined at a temperature of 650 K to be 8×10^{-11} and 3×10^{-10} ml molecule^{-1} sec^{-1}, respectively. The HBO_2 polymerization process appears to terminate with the trimer, however, and neither it nor the dimer appear to play an important role in the overall condensation process.

During the course of this work some additional experiments on dissociative electron attachment to HBO_2 and HCl were also performed to augment results obtained during prior ONR work. The data have been interpreted to yield a rate coefficient of 3.2×10^{-10} exp(-11,000/T) ml molecule^{-1} sec^{-1} for the reaction $e^- + HBO_2 \rightarrow BO_2^- + H$ and a value of 6×10^{-11} exp(-10,100/T) ml molecule^{-1} sec^{-1} for $e^- + HCl \rightarrow Cl^- + H$.

PREFACE

The author acknowledges the considerable experimental assistance of Dr. Robert K. Gould and Robert F. Burkert. Dr. Richard Miller of ONR is also due an expression of gratitude for his helpful discussions and timely support.

TABLE OF CONTENTS

		Page
	SUMMARY	1
	PREFACE	2
I.	INTRODUCTION	5
II.	ELECTRON ATTACHMENT	6
	A. Dissociative Attachment to HBO_2	6
	B. Dissociative Attachment to HCl	7
III.	BORON COMBUSTION PRODUCT CHEMISTRY	9
	A. Practical Considerations	9
	B. Apparatus	12
	1. The Low Pressure Flame Reservoir and Supersonic Jet	12
	2. Laser Light Scattering	14
	3. *Molecular Beam Mass Spectrometer*	16
	C. Results	20
	1. Laser Light Scattering Condensation Studies	20
	2. Mass Spectrometry	21
	D. Discussion	29
IV.	CONCLUSIONS AND RECOMMENDATIONS	37
V.	REFERENCES	39
	APPENDIX A: ELECTRON ATTACHMENT KINETICS IN FLAMES: DISSOCIATIVE ATTACHMENT TO HBO_2	
	APPENDIX B: ELECTRON ATTACHMENT KINETICS IN FLAMES: II. DISSOCIATIVE ATTACHMENT TO HCl	
	APPENDIX C: CHARGED SPECIES DIAGNOSTICS FOR COMBUSTION SYSTEMS	

LIST OF ILLUSTRATIONS

Figure		Page
1	APPARATUS FOR PARTICLE DETECTION VIA LASER LIGHT SCATTERING	15
2	SAMPLING CONE DESIGN	17
3	MOLECULAR BEAM MASS SPECTROMETER	19
4	SCATTERED LIGHT SIGNAL VS. BCl_3 FLOW	21
5	ION SPECTRUM FROM O_2-RICH FLAME JET	22
6	MB/MS RESPONSE AS FUNCTION OF TOTAL ADDED BORON	24
7	MB/MS RESPONSE TO B-CONTAINING SPECIES IN SUPERSONIC JET	25
8	MASS SPECTROMETER ION SOURCE PRESSURE AS FUNCTION OF JET POSITION AND AMBIENT PRESSURE	27
9	HBO_2 POLYMERIZATION AS FUNCTION OF JET FLOW TIME	33
10	PARTIAL HYPOTHETICAL POLYMERIZATION MECHANISM	36

LIST OF TABLES

Table		
1	AIR AUGMENTED SOLID PROPELLANT	11
2	LIQUID BORANE/AIR PROPELLANT	11
3	APPROXIMATE FLAME COMPOSITIONS, TEMPERATURES AND JET CONDITIONS	13
4	VALUES OF θ_{crit} FOR $\gamma_\infty = 1.4$	16
5	DISTRIBUTIONS OF B-CONTAINING PRODUCTS AFTER NOZZLE EXPANSION. FROZEN AND WITH AND WITHOUT CONDENSATION	30

I. INTRODUCTION

The primary goal of this research is the definition of the reaction mechanisms which link the large number of known boron combustion products, including condensed phases, to one another. During the early stages of the work, however, while the required instrumentation was being assembled and modified, additional experiments were performed to augment a body of data on electron attachment to HBO_2 and HCl which had been collected during earlier ONR and SAMSO work (Contracts N00014-74-C-0326 and F04701-72-C-0079, respectively). The results of these efforts are only summarized in the body of this report; details are available in the resultant publications included as Appendices A[1] and B.[2] The reprint of an invited review paper on charged species diagnostics in combustion systems prepared under the auspices of this contract for the 14th Aerospace Sciences Meeting of the AIAA is also included as Appendix C.[3]

---

1. Miller, W.J. and Gould, R.K., "Electron Attachment Kinetics in Flames: Dissociative Attachment to HBO_2," Chem. Phys. Lett. 38, 237-241 (1976).

2. Miller, W.J. and Gould, R.K., "Electron Attachment Kinetics in Flames: II. Dissociative Attachment to HCl," AeroChem TP-337, February 1976, submitted to J. Chem. Phys.

3. Miller, W.J., "Charged Species Diagnostics for Combustion Systems," AeroChem TP-331, AIAA Paper 76-135, presented at 14th AIAA Aerospace Sciences Meeting, Washington, DC, January 1976.

II. ELECTRON ATTACHMENT

A. DISSOCIATIVE ATTACHMENT TO HBO_2

Addition of boron compounds to high temperature combustion flames containing electrons gives rise to the formation of the negative ion BO_2^-. The thermodynamic properties of this ion were established[4,5] in our prior ONR-supported work and confirmed in subsequent studies by others.[6] Its electron affinity of 410 kJ $mole^{-1}$ (4.25 eV) renders it an attractive potential candidate for the control of electron densities in wakes and exhaust plumes as well as a considerable possible nuisance in MHD ducts. To quantitatively assess the effects of its formation in dynamic systems, however, the rate of its formation must be known in addition to its equilibrium properties. The rate coefficient for the dissociative attachment

$$e + HBO_2 \rightarrow BO_2^- + H \qquad (1)$$

was therefore measured in a number of standard, well characterized, laboratory test flames at total pressures of 0.13 and 1.0 atm. The data are consistent with the Arrhenius expression $k = 3.2 \times 10^{-10} \exp(-11{,}000/T)$ ml $molecule^{-1}$ sec^{-1} between 1730 and 2250 K. The failure of the observed BO_2^- formation rates to correlate in any systematic way with hypothetical three-body rate coefficients demonstrates that three-body attachment processes are negligible in these flames and that dissociative attachment dominates.

A more detailed account of these measurements may be obtained in Ref. 1, a reprint of which is included as Appendix A.

---

4. Jensen, D.E., "Electron Attachment and Compound Formation in Flames. I. Electron Affinity of BO_2 and Heats of Formation of Alkali Metal Metaborates," Trans. Faraday Soc. 65, 2123-2132 (1969).

5. Jensen, D.E., "Electron Attachment and Compound Formation in Flames. II. Mass Spectrometry of Boron-Containing Flames," J. Chem. Phys. 52, 3305-3306 (1970).

6. Srivastava, R.D., Uy, O.M., and Farber, M., "Effusion-Mass Spectrometric Study of the Thermodynamic Properties of BO^- and BO_2^-," Trans. Faraday Soc. 67, 2941-2944 (1971).

B. DISSOCIATIVE ATTACHMENT TO HCl

The highly electrophilic nature of chlorine coupled with its ubiquity render its negative ion chemistry the most important plasma processes in a wide variety of high temperature environments. Despite the obvious significance of Cl^- based on its thermochemical properties and high concentration in practical systems, there was, until this work, no direct measure available of its formation rate at high temperatures. Results of some of our prior work were therefore re-analyzed and supplementary experiments performed to determine the mechanism for Cl^- formation and the rate coefficient for the rate limiting step.

The experiments involve mass spectrometric measurements of negative ion concentrations as functions of flow time in the burnt gases of well characterized laboratory test flames seeded with small quantities of alkali metals and chlorine compounds. The results are consistent with the two-body dissociative attachment mechanism

$$e + HCl \rightarrow Cl^- + H \qquad (2)$$

with a rate coefficient well represented by the Arrhenius expression

$$k = 6 \times 10^{-11} \exp(-10{,}000/T) \text{ml molecule}^{-1} \text{ sec}^{-1} \qquad (3)$$

over the temperature range 1720 K to 2475 K. The flames are operated at pressures of 100 and 760 Torr. Electron concentrations were measured using a microwave resonance cavity method and positive ion profiles (total charged species) were determined with electrostatic probes. H-atom concentration profiles required to take account of the reverse detachment process are well known for the 760 Torr flames; in the low pressure flames they were obtained using a mass spectrometric negative ion tracer technique involving the known ion-molecule chemistry of molybdenum additives and confirmed via optical absorption measurements of [OH]. Contributions to Cl^- formation from three-body attachment processes are not observed. The measured values of k are found to be somewhat lower than, but in general agreement with, those inferred from

electron beam[7,8] and swarm studies[9] but are much lower than the values previously derived from measurements[10,11] of the reverse reaction rate.

The detailed description of this work is presented in Appendix B.[2] The manuscript is currently being revised somewhat and is expected to be accepted soon for publication in the Journal of Chemical Physics.

---

7. Buchel'nikova, I.S., "Cross Sections for the Capture of Slow Electrons by O_2 and H_2O Molecules and Molecules of Halogen Compounds," Sov. Phys. JETP 35, 783-791 (1959).

8. Azria, R., Roussier, L., Paineau, R., and Tronc, M., "Attachement Electronique Dissociatif sur HCl et DCl," Rev. Phys. Appl. 9, 469-473 (1974).

9. Christophorou, L.G., Compton, R.N., and Dickson, N.W., "Dissociative Electron Attachment to Hydrogen Halides and their Deuterated Analogs," J. Chem. Phys. 48, 1949-1955 (1968).

10. Howard, C.J., Fehsenfeld, F.C., and McFarland, M., "Negative Ion-Molecule Reactions with Atomic Hydrogen in the Gas Phase at 296°K," J. Chem. Phys. 60, 5086-5089 (1974).

11. Burdett, N.A. and Hayhurst, A.N., "Kinetics of Formation of Chloride Ions in Atmospheric Pressure Flames by Way of $HCl + e^- \rightleftarrows H + Cl^-$," Nature Phys. Sci. 245, 77-78 (1973).

III. BORON COMBUSTION PRODUCT CHEMISTRY

A. PRACTICAL CONSIDERATIONS

A good deal of work has been performed in the last decade on the thermochemistry of boron oxides and oxyhydroxides and on the overall kinetics of boron metal particle combustion (e.g. see Refs. 12-14). The stimulus for these efforts is the very attractive theoretical performance[15] of boron as a high energy propellant constituent. One critical aspect of our current knowledge of boron combustion chemistry, namely the kinetics and mechanisms of oxide and oxyhydroxide interconversion processes, remains poorly understood, however. It has been demonstrated[14] that the presence of water vapor above a burning boron particle greatly enhances product volatility and burning rate by converting liquid B_2O_3 on the surface to gaseous HBO_2. The interconversion of these two combustion products is also involved in important heat release processes which account for a significant portion of the potentially attainable propulsion performance. As noted above, the objective of the bulk of the research described in this report is the elucidation of the chemistry of these boron combustion products through an investigation of the mechanisms by which HBO_2 reacts to produce condensed phase products in propulsion system exhaust streams; the oxidation of the metal itself is not addressed in this work. However, it should be noted that many of the processes involved in these product interconversion mechanisms, or their reverse reactions, must also comprise important steps in metal combustion at higher temperatures.

---

12. Macek, A. and Semple, J.M., "Combustion of Boron Particles at Elevated Pressures," Thirteenth Symposium (International) on Combustion (The Combustion Institute, Pittsburgh 1971), pp. 859-868.

13. Macek, A. and Semple, J.M., "Combustion of Boron Particles at Atmospheric Pressure," Combust. Sci. Techn. 1, 181-191 (1969).

14. Roberts, R., "Boron Combustion: A Review," Proceedings of the 9th International Symposium on Space Technology and Science, Tokyo 1971, pp. 123-135.

15. All thermodynamic data taken from JANAF Thermochemical Tables, Dow Chemical Co., Midland, Mich.

The energetic implications of achieving the formation of condensed phase products, namely B_2O_3 in the liquid state, may be demonstrated by considering the thermodynamics of the alternative overall metallic boron oxidation schemes

$$2B + 2O_2 + H_2 \rightarrow 2HBO_2 \qquad \Delta H_{2000} = -275.4 \text{ kcal} \qquad (4)$$

$$2B + 2O_2 + H_2 \rightarrow B_2O_3(liq) + H_2O \qquad \Delta H_{2000} = -351.2 \text{ kcal} \qquad (5)$$

At a representative propulsion system exhaust temperature of 2000 K (that temperature for which these heat changes are given) the equilibrium constants (K_p) for these two processes are nearly identical and both products are therefore of nearly equal importance.* If condensation fails to occur and $B_2O_3(liq)$ is not formed, roughly half of the 76 kcal difference in these two pathways is not realized and the system suffers approximately a 10% decrease in overall performance. At lower exhaust temperatures the equilibrium concentrations of $B_2O_3(liq)$ are even higher with respect to HBO_2 and if condensation still does not occur, the loss of performance is correspondingly greater.

To further quantify these effects and determine their significance in practical systems, we have computed the specific impulse (I_{sp}), with and without B_2O_3 condensation, for several air augmented solid[16] and air breathing liquid[17] propellant systems under consideration[18] in the late 1960's.

---

* This is true only to a first approximation, of course; the exact ratio of these and other B-containing products at equilibrium depends on the detailed stoichiometry, B content, pressure, etc. of the entire system.

16. Deklau, B., et al, "Design Considerations for Air-Augmented Rocket Missiles and Related Afterburning Testing" (U), 3rd ICRPG/AIAA Solid Propulsion Conference (U), CPIA Publication No. 167, Vol. I, April 1968, pp. 481-500. (CONFIDENTIAL)

17. Rosenberg, S.D., Yates, R.E., and Adrian, R.C., "Secondary Combustion of Pentaborane - Hydrazine Exhaust in Air" (U), 10th Liquid Propulsion Symposium (U), CPIA Publication No. 176, Vol. I, October 1968, pp. 565-577. (CONFIDENTIAL)

18. Bubb, J.E., "Future Requirements--Airbreathing (U)," Propulsion Requirements for the 70's, AIAA 6th Propulsion Joint Specialist Conference, CPIA Publication No. 197, July 1970, pp. 13-58. (CONFIDENTIAL)

The conditions chosen for the performance calculations were flight Mach numbers 3.6 and 3.0 at 20,000 ft. altitude and a nozzle exhaust pressure of 7 psig (roughly ambient). The calculations were run with the Air Force Rocket Propulsion Laboratory (AFRPL) ISP Code which includes an air-augumentation routine. The results are summarized in Tables 1 and 2.

TABLE 1

AIR AUGMENTED SOLID PROPELLANT

Propellant:	$B_{1.0}C_{0.403}Cl_{0.42}Fe_{0.005}H_{0.755}N_{0.042}O_{0.170}$
Air/Propellant (wt):	10:1
Chamber Pressure (psia):	275
Flight Mach No.:	3.6
$I_{sp}^{(sec)}$ with B_2O_3 Condensation:	969
$I_{sp}^{(sec)}$ without Condensation:	905
Flight Mach No.:	3.0
$I_{sp}^{(sec)}$ with B_2O_3 Condensation:	1175
$I_{sp}^{(sec)}$ without Condensation:	1110

TABLE 2

LIQUID BORANE/AIR PROPELLANT

Propellant:	$B_{1.0}H_{3.81}N_{0.59}$
Air/Propellant (wt):	17:1
Chamber Pressure (psia):	75
Flight Mach No.:	3.6
$I_{sp}^{(sec)}$ with B_2O_3 Condensation:	585
$I_{sp}^{(sec)}$ without Condensation:	555
Flight Mach No.:	3.0
$I_{sp}^{(sec)}$ with B_2O_3 Condensation:	536
$I_{sp}^{(sec)}$ without Condensation:	517

A great many of these propellants, when tested, failed to achieve the 95-plus% efficiencies necessary for acceptable performance. It was found[16,17] that large air-propellant ratios were required to get good performance and the limitation was tacitly assumed to be tied to incomplete metal combustion. Analyses of the exhaust products, in the few cases where they were done,[17] indicate, however, that very little B_2O_3 (condensed) is present in the products. This strongly suggests that at least a portion of the poor performance is attributable to the product interconversion chemistry which is the subject of the present study.

The data of Tables 1 and 2 indicate decreases in system efficiencies of about 7 and 5% for the solid and liquid propellants, respectively. Typical experimental results produce deficiencies in the range 10%-15% or more at high boron loading levels. It thus appears that if the origin of the condensation losses could be identified and overcome, a substantial fraction of these inefficiencies could be eliminated.

B. APPARATUS

In these experiments, the burned gases from a number of $H_2/O_2/N_2$ flames containing BCl_3 additive are expanded through a nozzle and the characteristics of the supersonic jet emerging from the nozzle exit are examined as a function of added BCl_3. The use of a number of flames allows for variations in reservoir/jet temperatures and bulk gas chemical composition. Our effort comprised two sets of diagnostic procedures; (i) laser light scattering studies designed to define the limiting conditions for condensation and (ii) molecular beam mass spectrometry in boron-containing combustion product jets under conditions up to and including those defined in (i) above.

1. The Low Pressure Flame Reservoir and Supersonic Jet

The premixed flames which provide the reservoir section for the nozzle expansion are members of an extensive set of subatmospheric pressure, laminar $H_2/O_2/N_2$ flames used[2] in previous kinetic studies. They are supported in a Pyrex vacuum housing on an annular burner with an inner test flame matrix of 2.6 cm diam and an overall diameter of 4.5 cm. The unburned gas flow to

Table 3

APPROXIMATE FLAME COMPOSITIONS, TEMPERATURES AND JET CONDITIONS

(Reservoir Pressure, 150 Torr)

Flame	Unburned Gas Mole Ratios	Temperature K	Burned Gas Mole Fractions[a]							Jet Temperature K	Jet Pressure at Perfect Expansion Torr
			H_2O	H_2	O_2	H	OH	O	N_2		
F2	2.5/1.0/2.0	2120	4.4(-1)	1.1(-1)	b	2.6(-3)	1.3(-3)	b	4.4(-1)	1050	5.0
F3	2.5/1.0/3.0	1980	3.6(-1)	9.1(-2)	b	9.5(-4)	1.4(-3)	b	5.5(-1)	940	4.8
O2	3.4/1.0/2.0	1830	3.7(-1)	2.6(-1)	b	5.2(-4)	7.7(-6)	b	3.7(-1)	840	4.7
P3	3.5/1.0/3.0	1750	3.1(-1)	2.3(-1)	b	2.5(-4)	6.3(-6)	b	4.6(-1)	780	4.6
P6	3.5/1.0/6.0	1550	2.1(-1)	1.6(-5)	b	2.8(-5)	1.2(-6)	b	6.3(-1)	660	4.4
OO2	2.0/2.4/2.0	1780	3.7(-1)	3.2(-5)	2.6(-1)	5.6(-6)	1.8(-3)	7.9(-5)	3.7(-1)	840	4.8
OP3	2.0/2.5/3.0	1700	3.1(-1)	2.9(-5)	2.3(-1)	1.6(-6)	9.5(-4)	4.8(-5)	4.6(-1)	780	4.7
OU4	2.0/3.0/4.0	1500	2.5(-1)	5.4(-6)	2.5(-1)	b	4.2(-4)	1.0(-6)	5.0(-1)	710	4.6
OP6	2.0/2.5/6.0	1500	2.1(-1)	7.5(-5)	1.6(-1)	b	1.5(-4)	3.5(-6	6.3(-1)	650	4.4

[a] A(B) denotes A × 10^B

[b] denotes < 1.0(-6)

the burner is 20 to 30 ml(STP)sec^{-1} cm^{-2} (burner area). These flows provide stable flames in the 50-200 Torr pressure range. The unburned gas compositions of the test flame series, the individual temperatures as measured by Na D-line reversal and the computed burnt gas equilibrium compositions of each at the corresponding measured temperature are given in Table 3.

The BCl_3 additive is introduced into the center flame N_2 supply line from an inverted buret flow metering system. Ideally, gas flows are tailored so that only the central test flame combustion products enter the nozzle; the excess gas from the annular shield flame is pumped off through a bypass. This condition is not always attainable, however, and some dilution of the test gas by a portion of the shroud must be accepted when using lower velocity flames.

The nozzle through which the test flame combustion products are expanded is contoured to give a parallel, shock-free jet with a Mach number (M) of $\approx$ 3. Its exit-to-throat area ratio is 4.4, the throat area and throat-to-exit distance being 0.32 cm^2 and 1.6 cm, respectively. Typical ratios of chamber pressure to jet static pressure under conditions of perfect expansion are about 27 and the jet gas velocity is $\approx$ 1.6×10^5 cm sec^{-1}.

2. Laser Light Scattering

The presence of particulate material in the jet is monitored optically[19] by observing the light scattered by 90° from an incident laser beam. The optical apparatus configuration is shown in Fig. 1. The jet of combustion product gas issuing from the exit of the supersonic (Mach 3) nozzle is intersected by a chopped laser beam and the scattered light detected by an HTV R212 photomultiplier tube (PMT) focussed on the point of laser beam/jet intersection. The laser light at 732.8 nm is provided by a Spectra-Physics Model 133 He-Ne laser and is modulated at 1 kHz with a slotted disc rotating chopper. The PMT output signal is processed and displayed by a PAR Model 128 lock-in amplifier.

---

19. Stein, G.D. and Wegener, P.P., "Experiments on the Number of Particles Formed by Homogeneous Nucleation in the Vapor Phase," J. Chem. Phys. 46, 3685-3686 (1967).

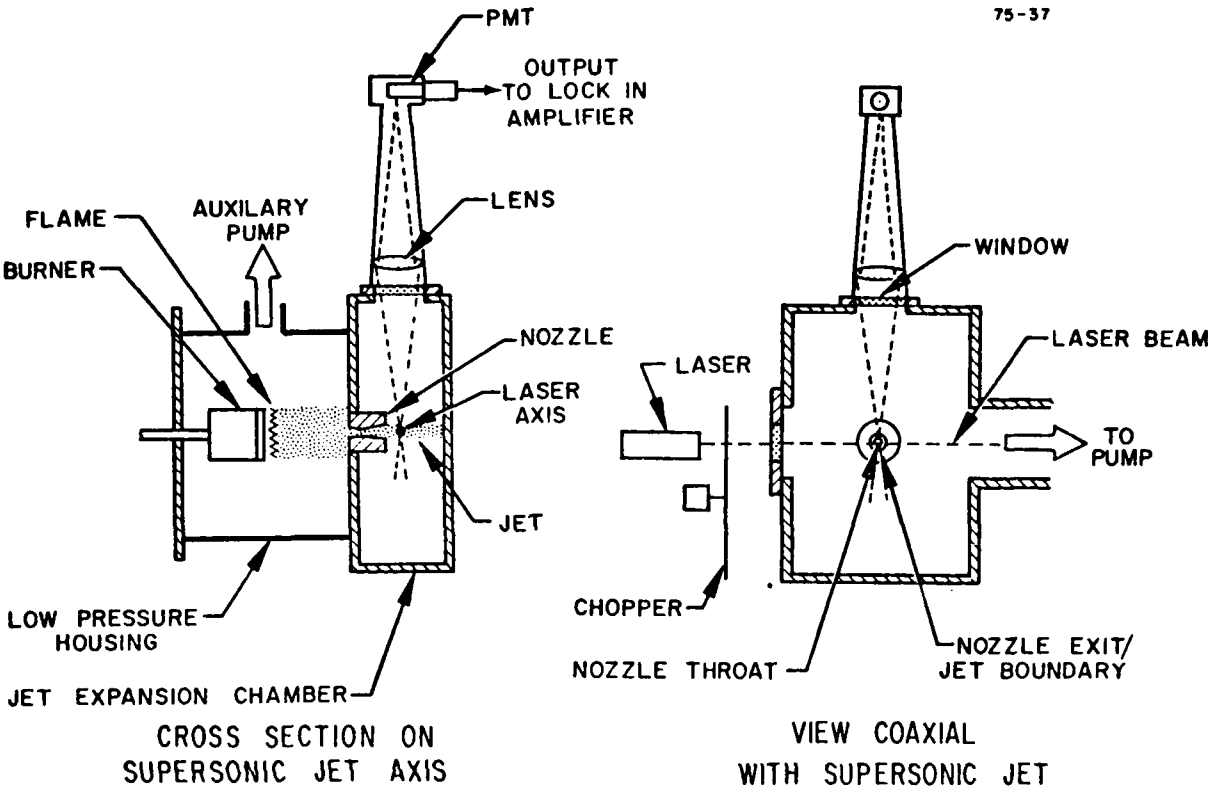

Fig. 1 APPARATUS FOR PARTICLE DETECTION VIA LASER LIGHT SCATTERING

Experimentally, the optical system was arranged geometrically and tested in the absence of a flame by entraining tobacco smoke in the burner chamber supply gas stream. The capability of the system to detect particles in actual combustion product mixtures was then established by seeding of $H_2/O_2/N_2$ or Ar flames with $Fe(CO)_5$. The burner housing in these tests was maintained at about 50 Torr and the static jet pressure is 1.5 ± 0.5 Torr.

The onset of condensation was readily observed as a distinct increase in the scattered light signal. The condensed phase material detected in this instance however is probably formed in the flame itself rather than in the nozzle during expansion; equilibrium calculations of the burnt gas composition indicate that the iron should be present in these flames largely as FeO(liquid) or Fe_3O_4(solid). Such is not the case for boron combustion products--thermodynamic considerations preclude the formation of

condensed phase boron oxides or acids anywhere but in the cooled gases downstream of the nozzle throat.

3. Molecular Beam Mass Spectrometer

The molecular beam/mass spectrometer apparatus employed in these studies was designed following what have become conventional procedures with the exception of the initial sampling stage. Since the gas to be sampled is present as a supersonic stream, the first inlet orifice must be designed to attach or swallow the shock created as the jet impinges upon it and thus allow for undisturbed sampling of the jet. For the inviscid continuum supersonic flow over a cone at zero angle of attack it is well known[20] that the shock wave enveloping the cone will be conical and attached to the cone tip only if the cone semi-angle does not exceed a critical value, θ_{crit}, which is a function only of the free stream Mach number and the specific heat ratio, γ, of the incident gas. For blunter cones the shock wave becomes detached (see Fig. 2a). Numerical values of θ_{crit} have been computed for $\gamma = 1.4$ with the results for 2 Mach numbers given in the first row of Table 4. Referring to these entries, it is clear that if we are interested in sampling in the Mach number range 2-3, the attached conical shock condition would only be met if the overall cone angle were less than about 40°. However, a sampling

TABLE 4

VALUES[a] OF θ_{crit} FOR $\gamma_\infty = 1.4$

Geometry	$M_\infty = 2$	$M_\infty = 3$
Cone (3)	40.6°	49.1°
Wedge (2)	23.0°	34.0°

[a]Estimated from Figs. 19 and 22 of Ref. 21.

20. Shapiro, A.H., The Dynamics and Thermodynamics of Compressible Fluid Flow (Ronald Press, New York, 1953), Vol. 1, Section 16.5, pp. 544-551.

21. Van Driest, E.R., "Basic Relations in Gas Dynamics," Handbook of Engineering Fundamentals, O.W. Eshbach, ed. (John Wiley, New York, 1953) 2nd Ed. Section 7, Part 7, pp. 7-08 - 7-39.

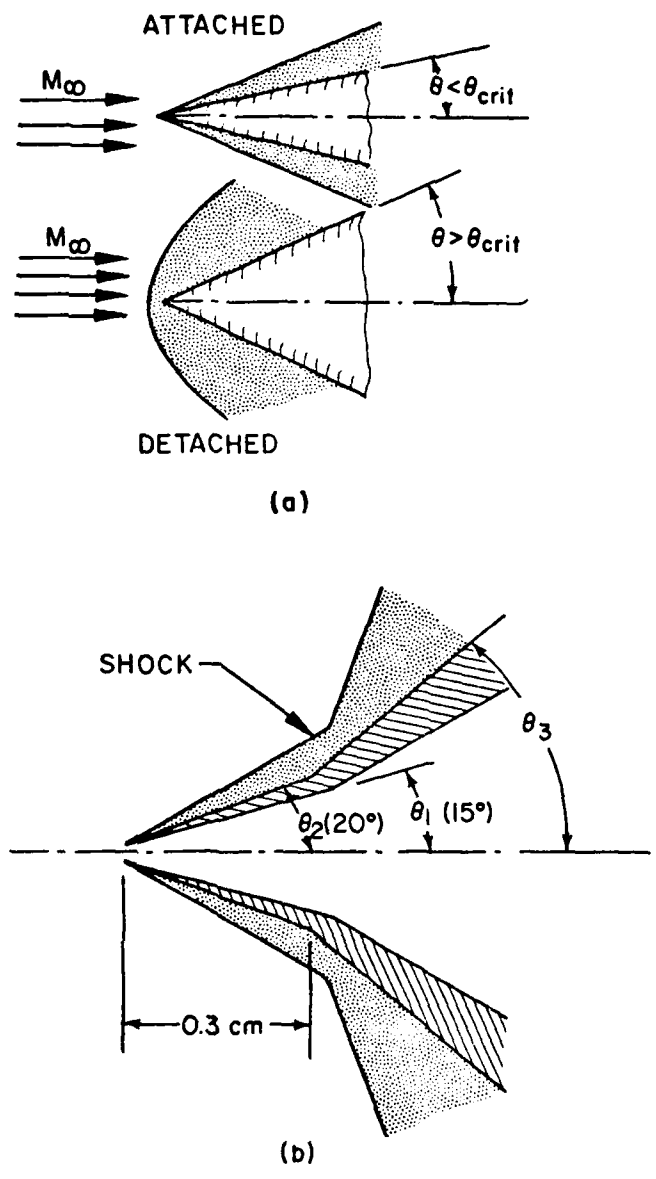

Fig. 2 SAMPLING CONE DESIGN

a. Cone/Shock Interactions
b. Experimental Configuration

cone must contain an orifice and, if we focus our attention in the immediate vicinity of the orifice, the flow more closely resembles (becomes asymptotically equivalent to) the flow over a two-dimensional wedge. Interestingly enough, supersonic flow over a wedge is qualitatively similar to that over a cone in that a critical wedge angle exists above which the flow will become detached. If one examines the computed values of θ_{crit} for the supersonic flow over a wedge (see row 2 of Table 4) it is found that they are significantly smaller at the same Mach number. Thus, again referring to Table 4, it is anticipated that the required cone angle in the immediate vicinity of the orifice would have to be kept below 23° in the Mach 2-3 range, but 'far' downstream from the orifice a cone angle of 40° would suffice. We are thus led to a configuration sketched in Fig. 2b which, in the absence of viscous flow effects, satisfies all of the attached shock conditions.

Prior work on ion sampling using cones of the above design has demonstrated[22] that, in practice, this ideal behavior is not achieved. However, the shock present at, or in the vicinity of, the sampling orifice has been found to be weak and to have little or no effect on the sample; this is apparently due to the low gas densities produced as the sample is re-accelerated from the region directly in front of the orifice.

The skimmer which excludes all but the central portion of the sampled gas stream is located, as shown in Fig. 3, between 100 and 200 cone orifice diameters downstream of the sampling inlet. The outside angle of the skimmer cone is 50°; the inside angle is 45°. The walls terminate at the cone tip in knife edges around a 0.25 mm diameter hole. Approximately 5 cm downstream of the skimmer opening, the beam is chopped with a normally closed tuning fork chopper (and collimated into an Extranuclear Model 041-1 co-axial electron impact ion source).

---

22. Burke, R.R. and Miller, W.J., "Study of Mass Spectrometric Ion Sampling Processes," Final Report, AeroChem TP-247, AFCRL-70-0550, DDC AD 725 149, September 1970.

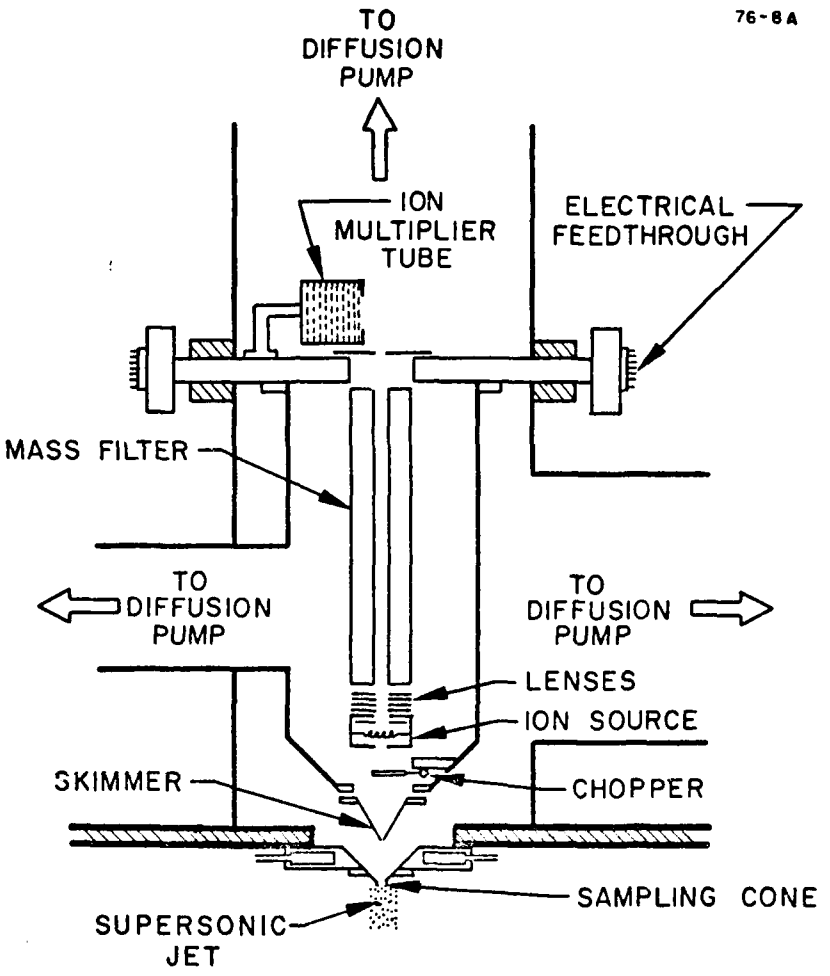

Fig. 3 MOLECULAR BEAM MASS SPECTROMETER

Following ionization, the sample ions are focussed and injected into the mass filter. The signal produced at the ion multiplier tube then feeds a lock-in amplifier and the signal is displayed on an oscilloscope or a strip chart recorder. The molecules originating in the sampling system are distinguishable as a 140 Hz a.c. signal superimposed (at most mass peaks) on a d.c. component resulting from the ionization of background gas in the ionizer. The a.c. sensitivity at any specific mass peak is dependent on the magnitude of this background and the identity of the gas but it typically ranges from about 10 parts per million (ppm) when no background is present to about 100 ppm where a large d.c. signal is present.

C. RESULTS

1. Laser Light Scattering Condensation Studies

The scattered light signal from the laser illuminated jet was determined as a function of BCl_3 loading in each of five of the test flames of Table 3; three O_2-rich flames and two H_2-rich analogues were utilized to provide a range of temperatures and variable gas composition. The two coolest flames, P6 (H_2-rich, $\sim$ 1550 K) and OP6 (O_2-rich, $\sim$ 1500 K) gave clear indications of particle formation at about 1% added BCl_3 in the test flame gas supply. In the three hotter flames, P3 (H_2-rich, 1730 K) OP3 (O_2-rich, 1700 K) and OU4 (O_2-rich, $\sim$ 1650 K), up to 9% BCl_3 was added without observing any significant scattered light.

Figure 4 shows some of the results of the light-scattering experiments conducted using the nozzle described in Section III.B. A burner housing pressure of 100 ($\pm$ 10) Torr and a static pressure of 2.0 ($\pm$ 0.3) Torr were used to insure overexpansion and thus minimize the possibility of interference from shock formation in the nozzle or along the jet axis between the exit plane and the laser/jet intersection point.

During the course of our early experiments, using a larger, 0.64 cm diam nozzle, under conditions of high BCl_3 addition rates, it was noted that deposits of white powdery condensate built up on the converging section of the nozzle inside the flame reservoir section and that particles were present at the cool outer boundaries of the shroud flame.

It was thus not certain whether all of the observed condensed phase was formed in the jet or whether some of it was formed within the reservoir housing. To remove this ambiguity, the 0.64 cm diam nozzle was replaced with one with a throat diam of 0.32 cm. The smaller nozzle (i) allows operation at higher burner pressures (which is advantageous from the point of view of promoting condensation) and (ii) allows a large amount of the burned gases to be pumped away through a bypass valve while only gases from the core of the flame pass through the nozzle. These two nozzles, although they necessitate the use of quite different reservoir and jet pressures and unburned flame gas

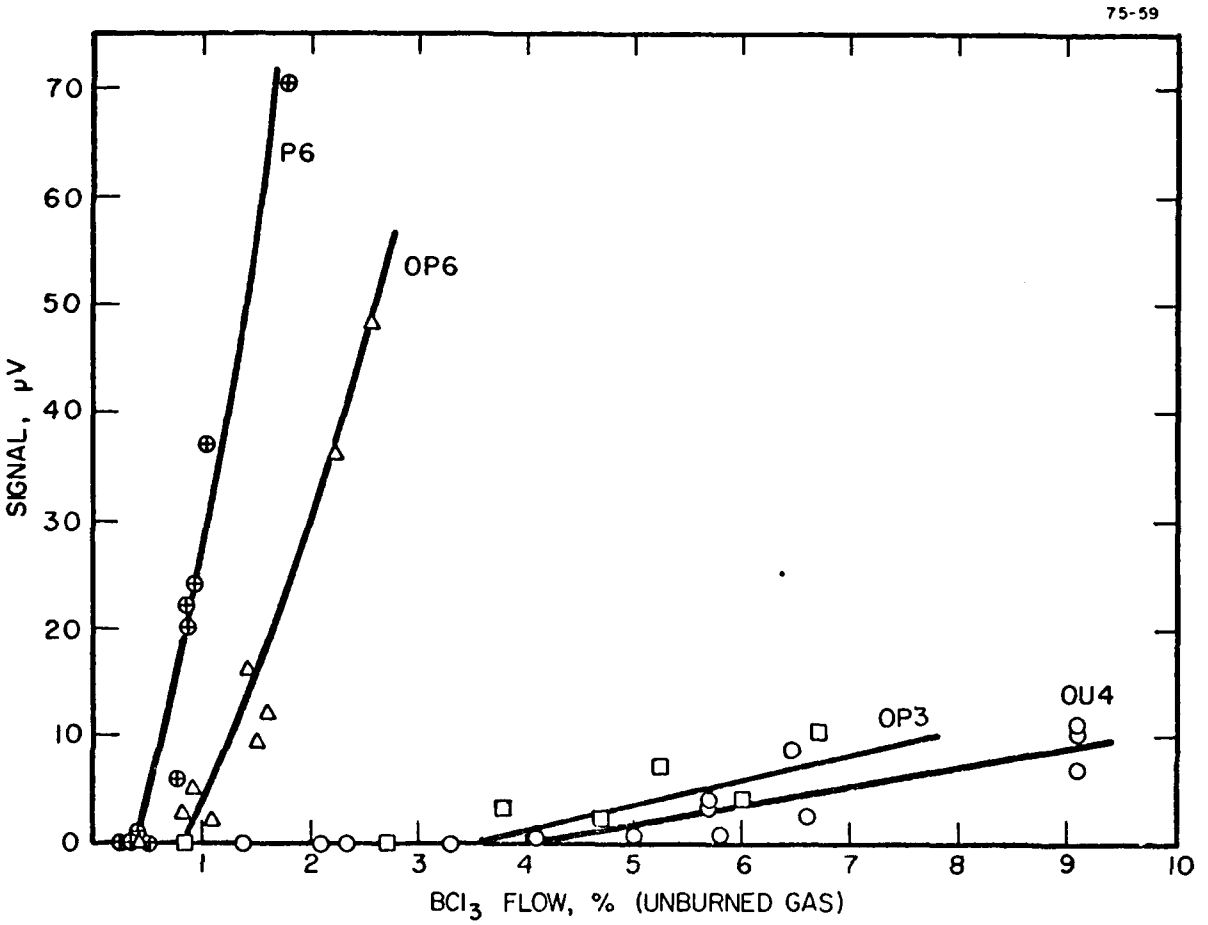

Fig. 4 SCATTERED LIGHT SIGNAL VS. BCl_3 FLOW

flow rates, yielded qualitatively similar results: condensation was readily induced in flames OP6 and P6 but was not observed in P3, OP3, or OU4. The small amounts of scattered light observed in the jets of the latter flames, which were reduced by using the smaller nozzle, are attributed to unwanted particle formation and ablation of condensate in the reservoir section--not to gas phase condensation anywhere in the test flame flow stream.

2. Mass Spectrometry

Supersonic jets produced by the expansion of many of the $H_2/O_2/N_2$ flames of Table 3 seeded with BCl_3 were examined mass spectrometrically. Upon the introduction of the BCl_3 to H_2-rich flames, ions at masses 35-38 and

42-45 are observed. These are attributed to the presence of Cl atoms (35 and 37), HCl (36 and 38) and/or HBO_2 (43 and 44), and $B(OH)_2$ (45 and 44). Whether BO_2 is present is uncertain; there is not enough data to quantitatively define the cracking patterns for HBO_2 and $B(OH)_2$ of which m/e = 43 and 42 may be part. In addition to these species, O_2-rich flames exhibit small concentrations of species at masses 51-55. Those may be due to ClO (51 and 53) and HOCl (52 and 54) although thermodynamic considerations predict very small concentrations ($< 10^{-5}$ mole fraction) of these species in the flame and throughout the nozzle expansion.

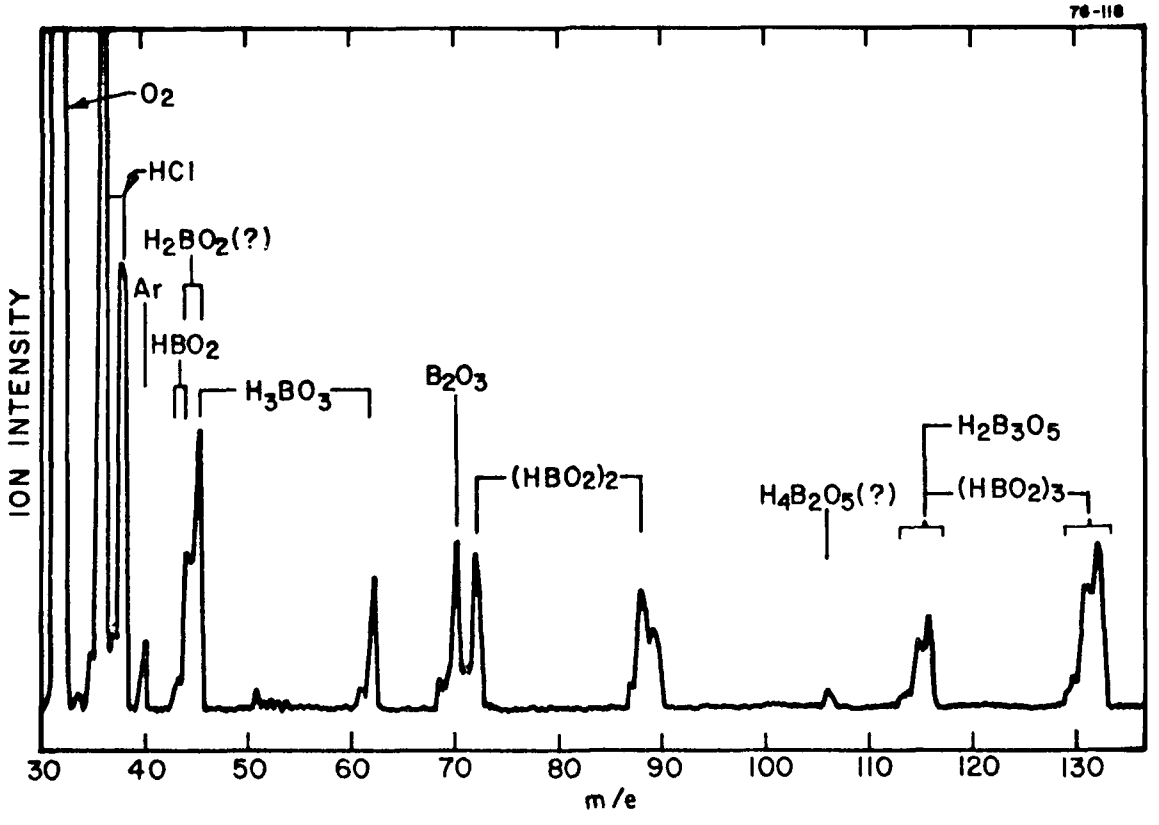

Fig. 5 ION SPECTRUM FROM O_2-RICH FLAME JET

Flame OF6, 0.5% BCl_3

Of the four test systems of Fig. 4, the jets produced by the two cooler flames, when supplied with amounts of BCl_3 below that required for condensation, exhibit a wider variety of boron combustion products and much lower concentrations of HBO_2 than do the hot flame jets. In addition to the species observed from the hot flames, ions appear at masses 70-72, 88, 89, 106, 113-115, and 130-132. An example of such an ion spectrum is given in Fig. 5. This data was taken at low mass spectrometer resolving power to enhance sensitivity and reduce mass discrimination effects in the mass filter but even so, most of the ions listed are separately observable.

The species giving rise to the observed ions have now been identified in nearly every case and some cracking patterns have been discerned. The trimer of HBO_2 has a complex cracking pattern at high ($\sim$ 70 V) ionizing energies, giving rise to ions throughout the groups about 114 and 131. Many of these fragment ions decrease in intensity or disappear rapidly, however, as ionizing energy is reduced and at 28 V, the energy at which the data of Figs. 5 to 7 were taken, fragmentation appears to be relatively unimportant. Mass 70 is certainly due to B_2O_3. It is not unambiguously clear how the ions at masses 72, 88, 89, and 106 are related to one another or, from what neutral species all of them are formed; from examination of ion spectra as a function of ionizing voltage, it appears that 88 and at least some of the signal at 72 are indicative of $(HBO_2)_2$ and that masses 89 and 106 arise from the adduct molecule $HBO_2 \cdot H_3BO_3$. Additional support for these contentions is derived from the fact that the intensities of masses 115 and 132, on the other hand, seem to be third order in added boron at low ionizing energy and therefore appear to contain three B atoms; mass 106 does not yield unambiguously to this analysis because of its relatively low signal level.

It appears quite clear from the data of Fig. 6 that mass 44 is first order in added boron and therefore contains but one B atom; similar plots (not shown) are obtained for mass 45. The relative abundances of these two ions vary considerably from flame to flame, however, and do not correlate at all with the isotopic distribution for boron assuming they both arise from the species H_2BO_2. Mass 44 is much (2-10 fold) more prevalent in hot O_2-rich flames and mass 45 becomes predominant at lower temperatures in H_2-rich environ-

ments. The behavior of mass 45 approximately parallels that of mass 62 which is attributed to H_3BO_3 on the basis of its observed first order dependence on added BCl_3. The ratio of the intensities of masses 45 and 62, however, is not

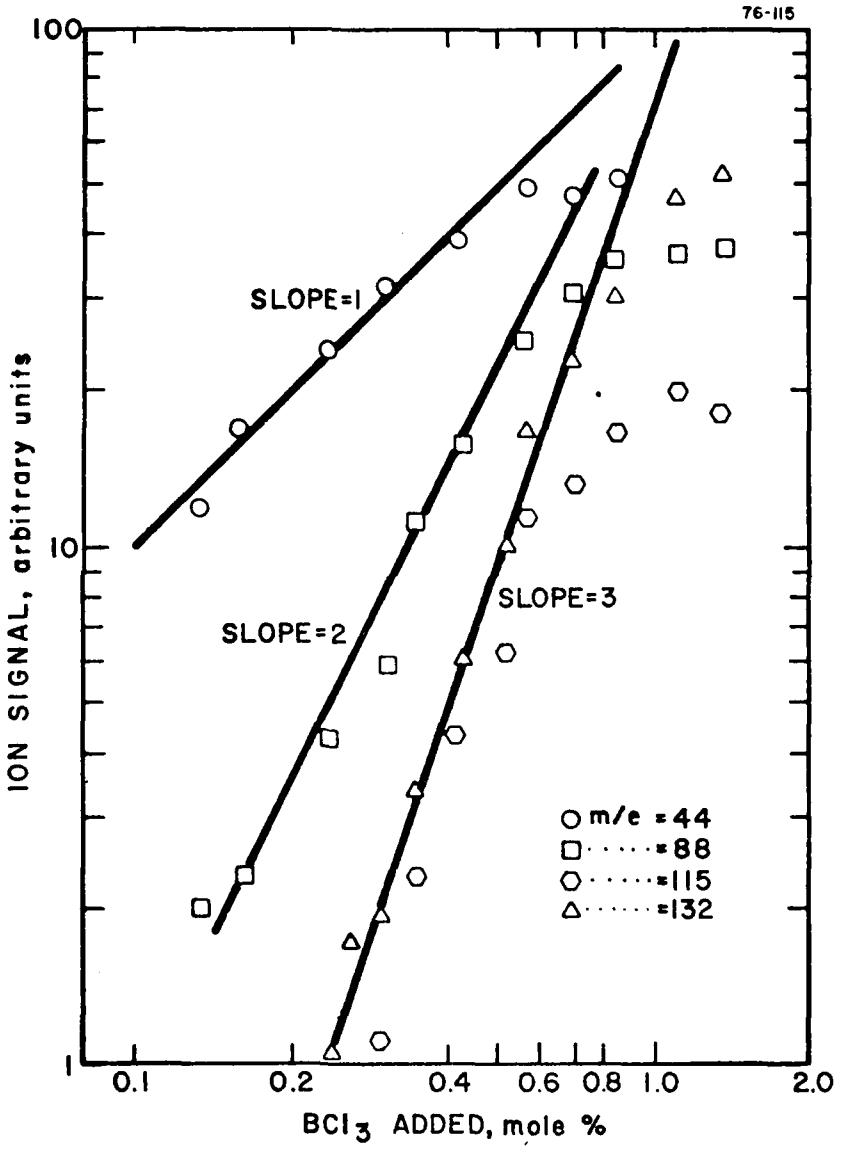

Fig. 6 MB/MS RESPONSE AS FUNCTION OF TOTAL ADDED BORON

Reservoir: Flame OP6, P = 150 Torr;
Jet: T = ~ 650 K, P = 4.0 Torr, data taken 3 cm downstream of nozzle exit.

strongly dependent on ionizing energy and if H_2BO_2 is an ion source fragment of H_3BO_3 the daughter ion is roughly 10 times more abundant than the parent over the ion source energy range 25-70 V. It seems more likely that the bulk of mass 45 is due to an actual neutral species H_2BO_2 rather than exclusively a daughter ion of H_3BO_3.

In principle it is possible to determine the number of boron atoms in a given species by examining the relative abundances of the isotopes within a group of ions. A molecule containing a single B atom will produce two ions at adjacent mass numbers, with the higher molecular weight being about four times more intense than the lower; two B atoms yield three adjacent peaks with relative abundances 4:31:66 in order of increasing mass; three B

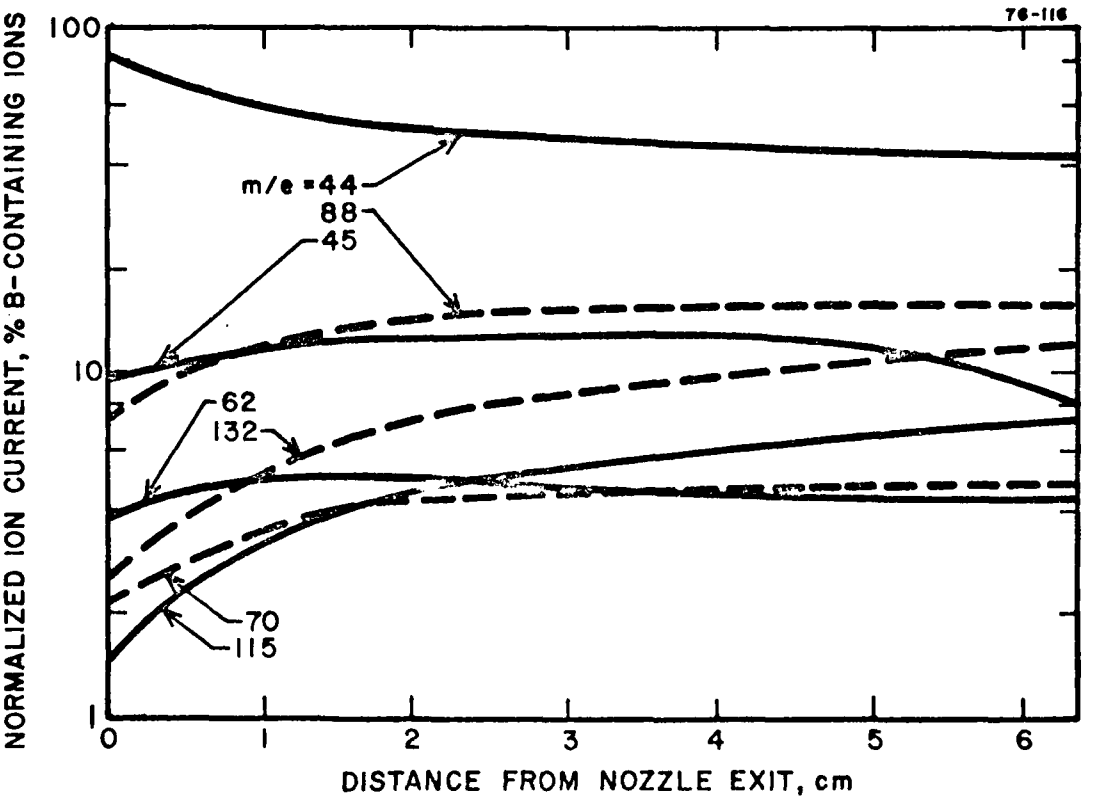

Fig. 7 MB/MS RESPONSE TO B-CONTAINING SPECIES IN SUPERSONIC JET

Reservoir: Flame OP6 = ∿ 1500 K, P = 150 Torr, BCl_3 = 0.6%;
Jet: T = ∿ 650 K, P = 4.5 Torr, velocity = 2.3 x 10^5 cm sec^{-1}

atoms, four peaks in the ratios 6:6:86:372:535. On this basis the ion spectrum in Fig. 5 is clearly indicative of three B-atom species at masses 131 ± 1 and 114 ± 1 although in both these cases the smallest ion in each set of four peaks (masses 129 and 112, respectively) is lost in the background noise. It is also apparent from Fig. 5 that two different species are responsible for the peaks at 88 ± 1, although here, too, the least intense components in the group are not visible. Unfortunately this analysis reveals nothing about the relative contributions of the two possible sources of mass 45; both the molecule H_2BO_2 and the daughter ion of H_3BO_3 contain only one B atom.

The data of Fig. 7 were obtained by traversing the nozzle over a 6 cm distance in front of the mass spectrometer sampling cone while maintaining the reservoir/nozzle exit pressure ratio required for perfect expansion. The burner-to-nozzle distance in the reservoir section of the system was held constant to avoid interference by kinetic effects in the flame gases upstream of the nozzle inlet. The exit pressure conditions required for perfect expansion of the jet were easily determined by monitoring the mass spectrometer ion source pressure as the nozzle exit-to-sampling cone distance was varied as shown in Fig. 8. Sizable excursions in the mass flow into the ion source are observed under both overexpanded and underexpanded conditions due to changes in gas density produced by the formation of shocks in the jet. As conditions for perfect expansion are approached, the magnitude of the pressure fluctuations decreases and the gas flow into the mass spectrometer becomes nearly constant throughout the length of the jet. In the flame jet of Fig. 8, this condition is closely approximated at an ambient (expansion chamber) pressure P_∞ = 5.7 Torr in fairly good agreement with the calculated value of 4.7 Torr given in Table 3 for fully frozen composition. It is also interesting to note that the apparent position of the first shock in the underexpanded flow at 1.5 Torr is located about 5 exit diameters (L/D) downstream of the nozzle. This compares quite well with a distance of 5.9 diameters predicted from the correlation

$$(L/D) = 0.67\ (Pres/P_\infty)^{1/2} \qquad (6)$$

where Pres is the combustion chamber pressure (150 Torr). The nozzle expansion and jet characteristics of even the smaller of our two nozzles appear therefore

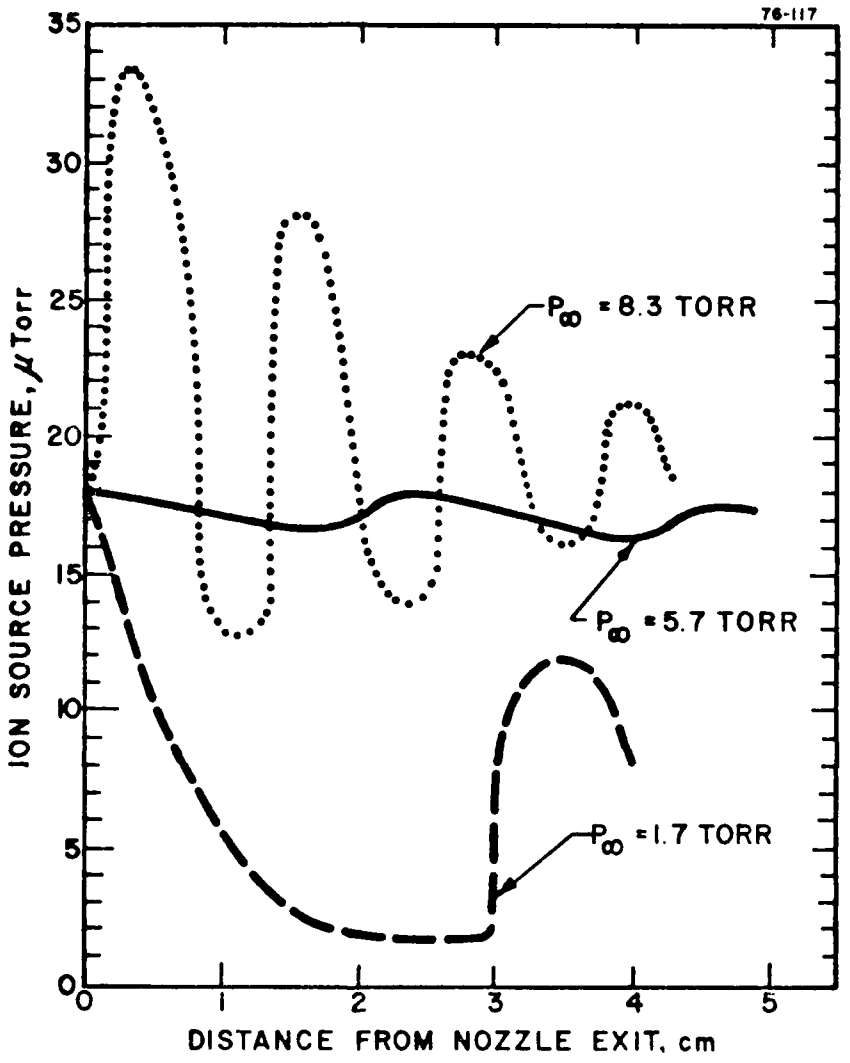

Fig. 8 MASS SPECTROMETER ION SOURCE PRESSURE AS FUNCTION OF JET POSITION AND AMBIENT PRESSURE

Reservoir: Flame OP3, P = 150 Torr

to be fairly close to those predicted on the basis of ideal behavior; undesirable boundary layer effects and complications due to shock formation within the nozzle are apparently unimportant. This is a very important observation since no attempt was made in this work to experimentally determine static temperatures in the supersonic jet and instead the temperatures were computed on the basis

of ideal gas dynamic behavior. The use of this assumption appears justified in view of the above and the jet temperature is therefore considered to be known as well as the measured flame temperatures in the reservoir section (typically, ± 40 K).

As the total boron concentration corresponding to the threshold of condensation is approached in the jets of the cooler flames, white, powdery boron deposits were observed to collect in two critical spots within the apparatus--the mass spectrometer sampling cone and the nozzle throat. Attempts to prevent this condensation on the sampling cone by electrically heating the lower section and base of the cone were only partially successful; as particles began to form in the jet, orifice clogging followed almost immediately and the experiment had to be interrupted for cleaning. Deposition of solids in the throat of the nozzle could be tolerated for longer periods of time. The immediate effect of this deposition is a decrease in effective throat diameter which alters the expansion ratio and mass throughput. This was reflected in steady, small changes in the jet pressure and was detectable as a decrease in the mass spectrometer ion source pressure. In order to minimize these problems, particularly near the condensation threshold where they were most severe, BCl_3 flow rates were first carefully set with the additive being dumped into the vacuum system downstream of the expansion chamber and then diverted into the flame for periods of only a few seconds during which specific ion current measurements were made.

From the data of Fig. 6, it is apparent that at total boron concentrations approaching 1%, species other than those cited must be produced; negative deviations from the direct integral order dependences indicated in Fig. 6 are observed for all species of mass 132 or less. Rapid, low resolution scans of the upper portion of the mass spectrum ($132 < m/e < 500$) under these conditions revealed peaks at the approximate masses 158, 185, 202, 230, 246, 274, 300, 315, 385, and 455. Efforts to determine the dependences of these species on added boron proved fruitless; the boron concentration range within which they were observable prior to orifice clogging was simply too small for meaningful measurements. The peaks identified were observed at an ionizer energy of 25 volts. No significant changes in the qualitative features of the

mass spectra were detected at energies up to 70 volts although very little effort was devoted to obtaining the high energy data.

At the lowest total boron concentration which yields detectable quantities of masses with 500 > m/e > 132, 158 and 230 are most intense. However, the ions within this entire mass range comprise only a small fraction of the total actually present. Turning off the quadrupole d.c. voltage at a fixed mass number setting allows all ions with masses equal to or greater than that value to be transmitted to the detector. By comparing the relative magnitudes of the signals for species above 132 and above 500, one obtains a measure of the proportion of high molecular weight species represented by the ions listed above, which are observable within the presently accessible mass range of the instrument. These tests reveal that, at the limit of detectability for ions with 132 > m/e > 500, the boron-containing species are partitioned as follows between various mass ranges: 40 < m/e < 140 = 30%; 140 < m/e < 500 = 10%; 500 < m/e = 60%. At higher boron concentrations, the higher molecular weight species comprise an extremely rapidly increasing proportion of the total.

D. DISCUSSION

At equilibrium, nearly all of the boron present in the jets of any of these flames would be in the form of liquid or solid B_2O_3. This is illustrated by the 'Complete Equilibrium' data given in Table 5 for two of the four tests systems--the jets of flame OP6 (which exhibits particle formation) and flame OP3 (which does not). The first attempt to interpret the results of our light scattering experiments was therefore based on a model involving homogeneous nucleation of B_2O_3. If it is assumed that the gas phase reactions occurring in the nozzle are very fast and that particle formation is limited by the rate of nucleation and condensation, the distributions of B-containing products in these two jets assume the values labeled 'Equilibrium, No Condensation' in Table 5. The resultant supersaturation ratios, S, for B_2O_3 have also been computed; they are simply the ratio of the 'No Condensation' values to those at 'Complete Equilibrium' (with liquid B_2O_3). It may be seen from these numbers that the less supersaturated of the two systems given is, in fact, the one which exhibits particle formation--the direct opposite of the result anticipated on the basis of the simple analysis. This inconsistency prevails in the

Table 5

DISTRIBUTIONS OF B-CONTAINING PRODUCTS AFTER NOZZLE EXPANSION
FROZEN AND WITH AND WITHOUT CONDENSATION

(Total B = 1 mole %, Reservoir P = 100 Torr)

	Complete Equilibrium		Equilibrium, No Condensation		Frozen, Chamber Composition	
Flame	OP6	OP3	OP6	OP3	OP6	OP3
$T_{(reservoir)}$, K	1500	1700	1500	1700	1500	1700
$T_{(nozzle\ exit)}$, K	650	780	650	780	650	780
Jet Mole Fractions						
HBO_2	1.3(-10)	7.5(-7)	7.7(-9)	3.6(-6)	1.0(-2)	1.0(-2)
BO_2	4.9(-14)	9.5(-12)	2.9(-12)	4.6(-11)	9.2(-6)	3.9(-5)
H_3BO_3	1.3(-6)	2.7(-4)	7.8(-5)	1.1(-3)	2.3(-6)	5.9(-7)
$(HBO_2)_3$	5.0(-8)	9.3(-5)	1.0(-2)	8.9(-3)	5.7(-9)	3.4(-11)
$B_2O_3(\ell)$	1.0(-2)	1.0(-2)	-----	-----	----	-----
Supersaturation Ratio	1.0	1.0	3.3	21	2.3(18)	1.1(10)

instances of the other two flame jets of Fig. 4; corresponding supersaturation values for flame jets P6 and OU4 are 8.2 and 27, respectively. Thus, the pair of systems with lowest S (3.3 and 8.2) produce particles and the two of highest S (21 and 27) do not.

An alternative possibility is that the nozzle chemistry is not fast, the extreme case in this instance being a nozzle exit composition frozen at the flame reservoir values. The mole fractions data in the 'Frozen Chamber Composition' columns of Table 5 are indicative of the jet compositions in this situation and it may be seen that the partial pressures of B_2O_3 are large compared to either of the other two cases. This abundance is reflected in the extremely large values of S which result. For the two flame jets P6 and OP6, $S = 6.7 \times 10^{18}$ and 2.3×10^{18}, respectively; for OP3 and OU4, $S = 1.1 \times 10^{10}$ and 3.0×10^{16}. In these frozen composition cases then, the relative supersaturation ratios are at least in the same order as the approximate tendency to exhibit condensation, i.e. P6 > OP6 > OP3 or OU4. Unfortunately, the S values are so large as to be meaningless with respect to assessing critical nucleus size. If it is assumed that $S = 10^{17}$ represents the critical super-

saturation and that the surface tension, σ, of the liquid B_2O_3 particle is $\approx$ 80 dynes cm^{-1}, then according to the Kelvin equation

$$r_c = \frac{2\,\sigma\,V}{kT\,\ln S} \qquad (7)$$

(where V is the B_2O_3 molecular volume) the radius of the critical nucleus, $r_c \leq 2.5 \times 10^{-9}$ cm at 700 K. This radius corresponds to a critical nucleus volume of 6.5×10^{-26} ml or about 10^{-3} B_2O_3 molecular volumes,* indicating that a single B_2O_3 molecule is already larger than the critical size for continuous growth.

Experimentally (see below) the exit plane composition is shown by the mass spectrometric results to lie intermediate between the 'Frozen' and 'Equilibrium, No Condensation' conditions displayed in Table 5--at least at total B concentrations where reproducible measurements could be made, viz., below those which induce particle formation (but well above saturation). This data together with the inconsistencies in the results of the analysis based on simple homogeneous nucleation of B_2O_3 makes it impossible to predict the conditions prerequisite to condensation from simple nucleation theories. The behavior of individual gas phase species as revealed by the mass spectrometric results provides far better indications of the mechanism involved.

Before venturing into the nature of the high molecular weight species which may ultimately lead to particle formation, a few comments concerning the simpler B-containing gaseous compounds are in order. The molecules HBO_2, B_2O_3, H_3BO_3 and $(HBO_2)_3$ are all observed in abundance. The presence of none of these in the supersonic jets is surprising; all are well-known gas phase species for which thermochemical data are available. The existence of H_2BO_2 (probably better written as $B(OH)_2$), $(HBO_2)_2$, $H_4B_2O_5$ and $H_2B_3O_5$ was not anticipated, however. Of these species only $B(OH)_2$ has been observed previously.[14] Unfortunately, there is little of a quantitative nature that can be done with these data; the systems of this study in which these new entities are observed are

---

* As is customary in such calculations, the molecular volume (V_m) is computed from condensed phase macroscopic density; i.e. $V_m = M/\rho N$ where M = molecular weight (69.6) and N is Avogadro's number.

in a severe state of disequilibrium so it is very perilous to attempt calculations of thermodynamic properties and the meager information on bulk gas free radical concentrations gives rise to large uncertainties in most attempted estimates of the individual rates of formation or decay of observed species. For reactions not involving bulk gas constituents, these uncertainties disappear, of course, and it becomes possible to estimate rates of such reactions subject only to the errors associated with the quantitative interpretation of the mass spectral data.

The polymerization of HBO_2 is unlikely to require the participation of a third body. In all likelihood, the energy released in the dimerization, which is probably of the order of 20-30 kcal,

$$2HBO_2 \rightarrow (HBO_2)_2 \qquad (8)$$

can be readily accommodated in the 18 vibrational and 3 rotational degrees of freedom available for a time long enough for collisional stabilization. Molecules of comparable complexity and even more stringent energy dissipation requirements frequently display second-order kinetics in this pressure range.[23] Therefore this reaction and the trimerization

$$(HBO_2)_2 + HBO_2 \rightarrow (HBO_2)_3 \qquad (9)$$

as well, are probably not pressure dependent* and the data of Fig. 7 may be employed to deduce rate coefficients for these processes directly from the partial pressures of the reactants. A linear replot of the mass spectrometer response to these three species as functions of reaction time (flow distance/jet velocity) is given in Fig. 9. The rate coefficient for Reaction (9), k_9, may be obtained directly by measuring the initial slope of the $(HBO_2)_3$ profile and dividing it by the product $[HBO_2][(HBO_2)_2]$. Implicit in this procedure are the assumptions that: (1) Reaction (9) is the only source of the trimer, (2) at t = 0, the rate of the reverse of Reaction (9) is negligible

---

* This point could be readily checked by varying jet static pressure. Unfortunately since the determination of these rate coefficients was not the major thrust of this effort, time did not permit the execution of such experiments.

23. Benson, S.W., The Foundations of Chemical Kinetics (McGraw Hill, New York, 1960), Chaps. XI and XII.

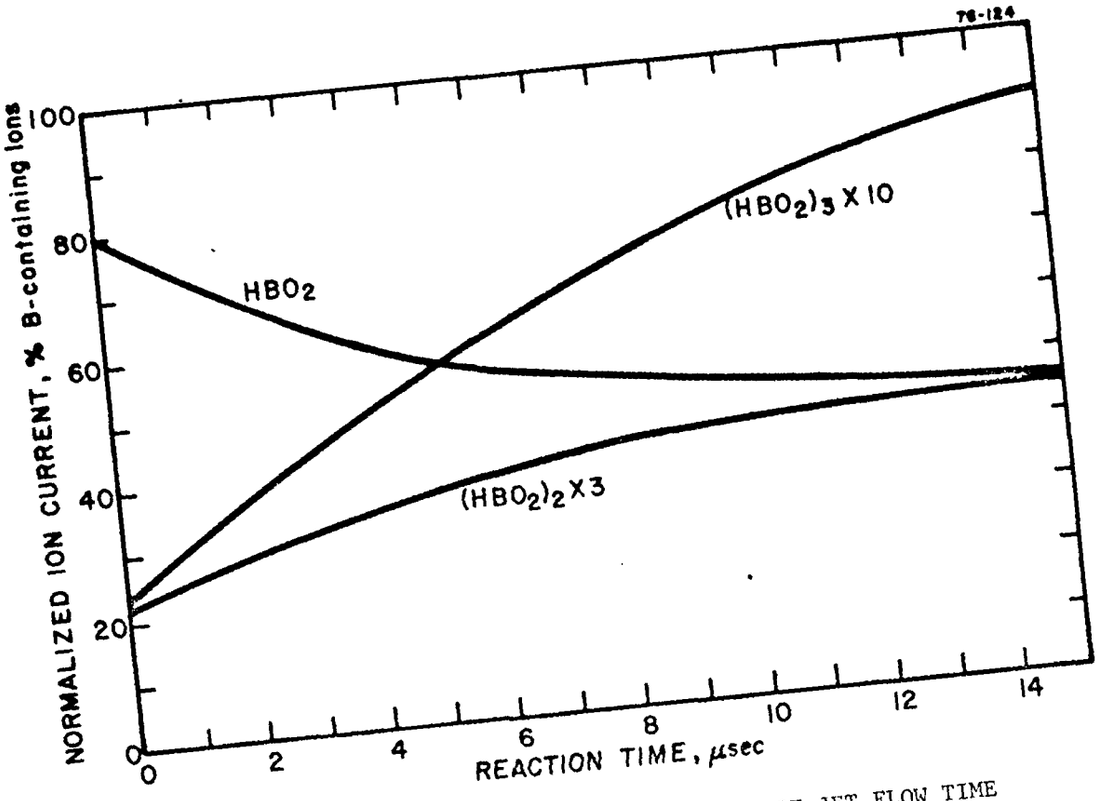

Fig. 9 HBO_2 POLYMERIZATION AS FUNCTION OF JET FLOW TIME (conditions as in Fig. 7)

compared to its forward rate, and (3) the HBO_2 and $(HBO_2)_2$ ion currents are a direct measure of the corresponding species concentrations in the jet. The first two of these assumptions are considered quite reasonable; the third is subject to considerable potential error due to the complete lack of knowledge of relative ionization cross sections and, to a lesser extent, other instrumental mass discrimination effects. These errors are operative in the estimation of the rate coefficient, k_8, as well.

Assuming that Reactions (8) and (9) are the only source and sink, respectively, for $(HBO_2)_2$ leads to the following expression for its rate of change:

$$d[(HBO_2)_2]/dt = k_8[HBO_2]^2 - k_9[HBO_2][(HBO_2)_2] \quad (10)$$

The left-hand side of this expression may be obtained directly from Fig. 9. Then adopting assumption (3), above, concerning the concentrations and ion current relationships and using the computed local values of k_9 one obtains values for k_8 throughout the jet. The constancy of these results over the range of flow times for which data are available is a qualitative measure of the validity of the mechanistic model. If other processes intervened significantly, it would be extremely fortuitous if the derived values for k_8 were constant over an appreciable distance or time. In fact, these calculations produce numbers with positive and negative deviations no larger than 15% of the average for the first 1.2×10^{-5} sec of flow time after which a distinct decrease in the results is observable. The latter effect is probably due to either or both reactions approaching equilibrium and the onset of either or both of the reverse reactions. The values for these two rate coefficients at the early flow times, where they should be most accurate, are given by

$$k_8 = (8.1 \pm 1.0) \times 10^{-11} \text{ ml molecule}^{-1} \text{ sec}^{-1} \quad (11)$$

$$k_9 = (3.0 \pm 1.0) \times 10^{-10} \text{ ml molecule}^{-1} \text{ sec}^{-1} \quad (12)$$

at a jet temperature of 650 K and an average $[HBO_2] \approx 2 \times 10^{-14}$ ml^{-1}.

The absence of higher polymers of HBO_2 from the ion spectrum under any conditions seems to indicate that the trimer formation is a mechanistic dead-end. This is also inferred from the persistence of a third order dependence of $(HBO_2)_3$ on added boron at relatively large addition rates; many other species including B_2O_3, H_3BO_3 and, most notably, the entity with mass 115 ($H_4B_2O_5$) exhibit deviations from integral value dependences on additive at concentrations significantly below the points at which $(HBO_2)_3$ begins to deviate; this is illustrated by the points corresponding to mass 115 in Fig. 6. Behavior of this kind sets in as chemical reactions which act as a sink for the species in question become important; the kinetic expression for their steady-state concentration is then no longer simply a function directly proportional to precursor concentrations. The $(HBO_2)_2$ (88) curve in Fig. 6 illustrates this point in that it departs from second order dependence on HBO_2 at additive levels where $(HBO_2)_3$ formation becomes a significant sink via Reaction (9), i.e., when the second term on the right-hand side of Eq. (10) becomes significant.

A corollary of this argument is that those species which exhibit deviations from simple integral kinetic dependences at the lowest additive concentrations are the species which undergo further reaction most readily. It is among these species that the mechanistic pathway to the high molecular species, which comprise 'pseudo-condensation nuclei', must be sought. Further clues as to the identity of these critical nucleation precursors may be obtained from the molecular weights of the species observed at high (near-condensation onset) total boron concentrations. Considering the abundant simpler molecules HBO_2, H_3BO_3 and B_2O_3 as monomers in the vocabulary of classical nucleation schemes, one may subtract the respective molecular weights, 44, 62 and 70 from the observed higher mass species to deduce the identity of the molecule to which they adhere. For example, in the instance of the polymer with mass 158 to 160 (identified nominally as mass 158 in Section III.C.2 above), the possible origins are 44 + 115 ($HBO_2 + H_2B_3O_5$), 70 + 88 ($B_2O_3 + (HBO_2)_2$), and 63 + 95. Since the low molecular weight spectrum does not reveal any constituent with mass 95 and since the dimer, $(HBO_2)_2$, appears to be nicely accounted for in the trimer formation scheme, the first of the three possibilities appears by far the most likely. Reinforcing this hypothesis is the observation that $H_2B_3O_5$ (115) begins to deviate from linear behavior in Fig. 6 relatively early indicating its significant participation in some reaction which depletes its concentrations.

Analogous arguments when applied to other observed polymeric molecules lead to the mechanistic hypothesis partially outlined in Fig. 10. This reaction scheme accounts for all the species observed in this work but is, by no means, the only possible route for their formation. For example, at some stage in the polymerization the interactions between two entities each containing more than three B atoms surely become important and the reactions postulated will be bypassed. Similarly, the reactions written are not meant to uniquely and exclusively define the elemental steps involved; for example, the addition of HBO_2 as written in several instances may well be the combined result of H_3BO_3 addition accompanied or followed immediately by elimination of a molecule of H_2O. The intermediate adduct in this case would be too unstable to survive electron impact ionization or be of such short-lived duration as to render its steady state concentration too low for detection.

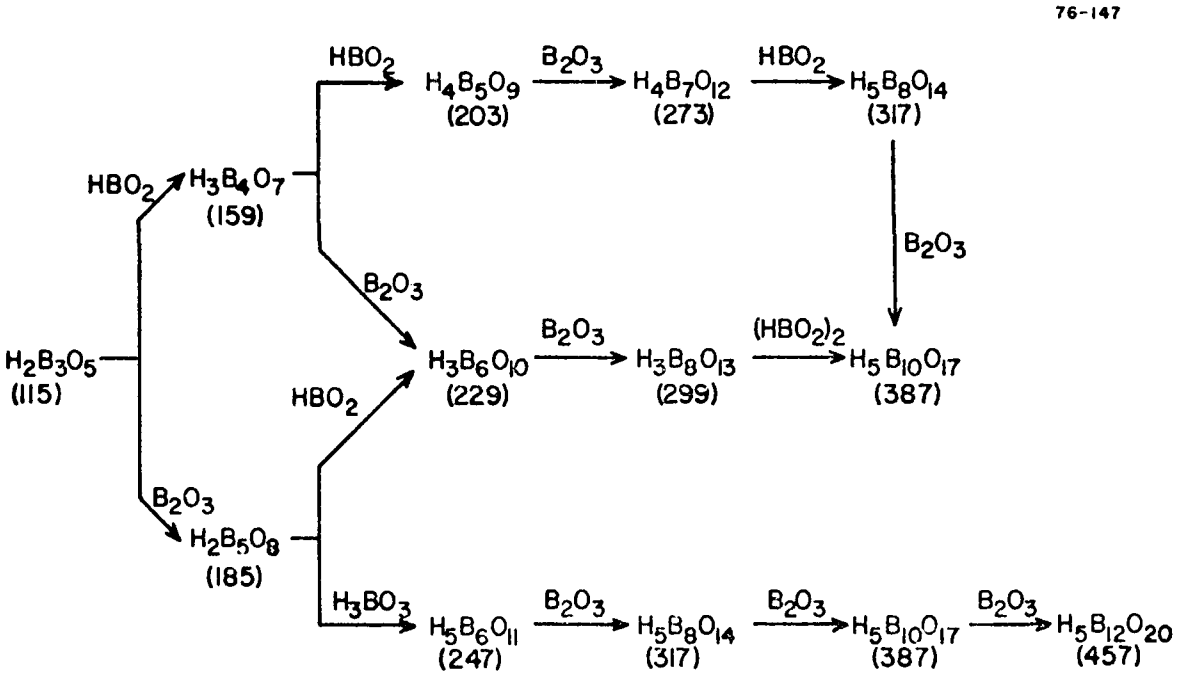

Fig. 10 PARTIAL HYPOTHETICAL POLYMERIZATION MECHANISM

However, despite these uncertainties, the picture which emerges from this analysis, strongly indicates that there is no distinct step that can be identified with dehydration and that no single monomeric species can be isolated upon which to base a simple model. As the scheme in Fig. 10 progresses from left to right, the proportion of boron in the observed species gradually increases implying the progressive elimination of H_2O. The fact that a series of polymers separated by 18 mass units is not observed would seem to indicate that the dehydration occurs predominantly among the lower molecular weight species, i.e., via the simple reactions interconnecting HBO_2, H_3BO_3, B_2O_3, etc. It is possible, though, that the members of these series other than those observed are simply present at concentrations too low for detection. The model is unfortunately not yet complete.

IV. CONCLUSIONS AND RECOMMENDATIONS

It has been demonstrated that the energetically important condensation of boron combustion products cannot be accurately predicted from models based on simple homogeneous nucleation theory. Mass spectrometric examination of systems actually undergoing nucleation reveal that the reaction mechanisms by which HBO_2 is converted to condensed phase B_2O_3 are extremely complex and that a number of 'monomeric' species are involved. The essential process--that of the elimination of H_2O--occurs gradually rather than at any discreet point or over any limited range of polymer molecular weights. A complex array of intermediate polymeric species with widely variable H/O/B proportions is present in these dynamic condensing combustion product gas streams. The reactions leading to the formation of the dimer and trimer of HBO_2, although readily anticipated on intuitive and thermochemical grounds do not appear to be essential steps in the overall process leading to the production of condensed phases. Rate coefficients for these two reactions, viz.,

$$2HBO_2 \rightarrow (HBO_2)_2$$

and

$$HBO_2 + (HBO_2)_2 \rightarrow (HBO_2)_3$$

have been measured here at a temperature of 650 K as 8×10^{-11} and 3×10^{-10} ml molecule^{-1} sec^{-1}, respectively. However the portion of the overall mechanism which they comprise appears to be incidental in the overall scheme; as nucleation proceeds, these dimers and trimers may well become involved but other reactions appear to play a much more significant role in the production of higher molecular weight species.

It is quite likely that complicated phenomena of the sort encountered in the study are operative in a great many other practical systems as well. There are, in fact, very few real-life situations to which one may apply conventional nucleation theories with much prospect of attaining accurate predictions due to an almost certain knowledge of the complexity of the chemistry involved. The work performed on this contract, although it does not yet provide a complete picture of boron oxide nucleation, demonstrates that the chemistry of such processes can be explored in great detail even in situations where the overall chemical composition is quite complex.

To complete the effort initiated with this study, the experimental capability of the molecular beam mass spectrometer should be extended to higher mass numbers to facilitate examination of the later stages of nucleation and particle growth. This work should also include an investigation of the effects of additives or potential fuel impurities which might accelerate the nucleation and/or particle growth processes. Candidate 'catalysts' include charged species which may induce heterogeneous ionic nucleation and/or more easily condensed materials such as silicates which may serve as nuclei for boron combustion products by virtue of their mutual liquid phase solubilities. If any of these effects prove significant it may be possible, through the inclusion or elimination of a relatively small amount of added material to effectively control particle and smoke formation via alteration of condensation kinetics. The instrumental aspects of this extended work are straightforward; however, several system modifications including jet expansion to lower pressures and enlargement of the first stage sampling capacity are indicated.

The systems amenable to investigation via the techniques employed in this work are by no means limited to supersonic jets containing metal oxides. In principle, a wide variety of other nucleation problems of considerable practical importance could be attacked including those associated with the formation of atmospheric aerosols, condensation induced by the interaction of more conventional exhaust products with air and smoke formation--whether intentional or accidental. The essential experimental features of the approach to be taken in all of these cases would be the same as those employed in the present work. Specific sampling system parameters, mass spectrometer response characteristics and the design of the apparatus in which the nucleation/condensation processes are induced would be tailored to the particular needs of the study to be undertaken.

V. REFERENCES

1. Miller, W.J. and Gould, R.K., "Electron Attachment Kinetics in Flames: Dissociative Attachment to HBO_2," Chem. Phys. Lett. 38, 237-241 (1976).

2. Miller, W.J. and Gould, R.K., "Electron Attachment Kinetics in Flames: II. Dissociative Attachment to HCl," AeroChem TP-337, February 1976, submitted to J. Chem. Phys.

3. Miller, W.J., "Charged Species Diagnostics for Combustion Systems," AeroChem TP-331, AIAA Paper 76-135, presented at 14th AIAA Aerospace Sciences Meeting, Washington, DC, January 1976.

4. Jensen, D.E., "Electron Attachment and Compound Formation in Flames. I. Electron Affinity of BO_2 and Heats of Formation of Alkali Metal Metaborates," Trans. Faraday Soc. 65, 2123-2132 (1969).

5. Jensen, D.E., "Electron Attachment and Compound Formation in Flames. II. Mass Spectrometry of Boron-Containing Flames," J. Chem. Phys. 52, 3305-3306 (1970).

6. Srivastava, R.D., Uy, O.M., and Farber, M., "Effusion-Mass Spectrometric Study of the Thermodynamic Properties of BO^- and BO_2^-," Trans. Faraday Soc. 67, 2941-2944 (1971).

7. Buchel'nikova, I.S., "Cross Sections for the Capture of Slow Electrons by O_2 and H_2O Molecules and Molecules of Halogen Compounds," Sov. Phys. JETP 35, 783-791 (1959).

8. Azria, R., Roussier, L., Paineau, R., and Tronc, M., "Attachement Electronique Dissociatif sur HCl et DCl," Rev. Phys. Appl. 9, 469-473 (1974).

9. Christophorou, L.G., Compton, R.N., and Dickson, N.W., "Dissociative Electron Attachment to Hydrogen Halides and their Deuterated Analogs," J. Chem. Phys. 48, 1949-1955 (1968).

10. Howard, C.J., Fehsenfeld, F.C., and McFarland, M., "Negative Ion-Molecule Reactions with Atomic Hydrogen in the Gas Phase at 296°K," J. Chem. Phys. 60, 5086-5089 (1974).

11. Burdett, N.A. and Hayhurst, A.N., "Kinetics of Formation of Chloride Ions in Atmospheric Pressure Flames by Way of $HCl + e^- \rightleftarrows H + Cl^-$," Nature Phys. Sci. 245, 77-78 (1973).

12. Macek, A. and Semple, J.M., "Combustion of Boron Particles at Elevated Pressures," Thirteenth Symposium (International) on Combustion (The Combustion Institute, Pittsburgh 1971), pp. 859-868.

13. Macek, A. and Semple, J.M., "Combustion of Boron Particles at Atmospheric Pressure," Combust. Sci. Techn. 1, 181-191 (1969).

14. Roberts, R., "Boron Combustion: A Review," Proceedings of the 9th International Symposium on Space Technology and Science, Tokyo 1971, pp. 123-135.

15. All thermodynamic data taken from JANAF Thermochemical Tables, Dow Chemical Co., Midland, Mich.

16. Deklau, B., et al, "Design Considerations for Air-Augmented Rocket Missiles and Related Afterburning Testing" (U), 3rd ICRPG/AIAA Solid Propulsion Conference (U), CPIA Publication No. 167, Vol. I, April 1968, pp. 481-500. (CONFIDENTIAL)

17. Rosenberg, S.D., Yates, R.E., and Adrian, R.C., "Secondary Combustion of Pentaborane - Hydrazine Exhaust in Air" (U), 10th Liquid Propulsion Symposium (U), CPIA Publication No. 176, Vol. I, October 1968, pp. 565-577. (CONFIDENTIAL)

18. Bubb, J.E., "Future Requirements--Airbreathing (U)," Propulsion Requirements for the 70's, AIAA 6th Propulsion Joint Specialist Conference, CPIA Publication No. 197, July 1970, pp. 13-58. (CONFIDENTIAL)

19. Stein, G.D. and Wegener, P.P., "Experiments on the Number of Particles Formed by Homogeneous Nucleation in the Vapor Phase," J. Chem. Phys. 46, 3685-3686 (1967).

20. Shapiro, A.H., The Dynamics and Thermodynamics of Compressible Fluid Flow (Ronald Press, New York, 1953), Vol. 1, Section 16.5, pp. 544-551.

21. Van Driest, E.R., "Basic Relations in Gas Dynamics," Handbook of Engineering Fundamentals, O.W. Eshbach, ed. (John Wiley, New York, 1953) 2nd Ed. Section 7, Part 7, pp. 7-08 - 7-39.

22. Burke, R.R. and Miller, W.J., "Study of Mass Spectrometric Ion Sampling Processes," Final Report, AeroChem TP-247, AFCRL-70-0550, DDC AD 725 149, September 1970.

23. Benson, S.W., The Foundations of Chemical Kinetics (McGraw Hill, New York, 1960), Chaps. XI and XII.

APPENDIX A

Volume 38, number 2 CHEMICAL PHYSICS LETTERS 1 March 1976

ELECTRON ATTACHMENT KINETICS IN FLAMES: DISSOCIATIVE ATTACHMENT TO HBO_2

William J. MILLER and Robert K. GOULD
AeroChem Research Laboratories, Inc., Princeton, New Jersey, USA

Received 22 October 1975

The rate coefficient for the dissociative electron attachment $e + HBO_2 \rightarrow BO_2^- + H$ has been measured in a number of well characterized laboratory test flames at total pressures of 1.0 and 0.13 atm. The data are consistent with the Arrhenius expression $k = 3.2 \times 10^{-10} \exp(-11000/T)$ ml molecule^{-1} s^{-1} between 1730 and 2250 K. The failure of the observed BO_2^- formation rates to correlate in any systematic way with hypothetical three-body rate coefficients demonstrates that three-body attachment processes are negligible in these flames and that dissociative attachment dominates.

1. Introduction

In recent years a number of thermochemical studies have shown that the oxides and oxyhydroxides of boron [1,2] and a number of transition metals [3–5] have electron affinities as great or greater than those of the halogens. The abilities of these metal-containing compounds to form stable negative ions at high temperatures make them of considerable interest in combustion plasmas such as MHD channel flows and rocket exhausts where the concentrations of free electrons are important. Although these studies have resulted in the generation of the thermochemical data necessary to assess the equilibrium effects of these electrophilic compounds, kinetic information is still lacking. The work described here comprises the first measurements of the rate coefficient for the reaction

$$e + HBO_2 \rightarrow BO_2^- + H\,. \qquad (1)$$

The measurements were performed in a number of well-characterized laboratory combustion flames spanning the temperature range 1730–2250 K at pressures of 1.0 and 0.13 atm (100 torr).

2. Experimental

Due to the possibility of interference in the measurements of k_1 by three-body electron attachment reactions it was deemed desirable to perform measurements of BO_2^- formation rates in both 1 atm and low pressure flames. The 1 atm flames used are the same $H_2/O_2/N_2$ systems employed in prior thermodynamic work [1–6]. The concentration profiles for all the important neutral constituents (H_2O, H_2, H, OH) as functions of flow or reaction time in these flames are thus available from these and other previous studies and no further work of this nature was required at 1 atm. Typically, the results of these concentration measurements span reaction times from 0.5 to 5 ms – an interval adequate for the boron-containing species of this study to reach near-equilibrium concentrations. Unfortunately, very little neutral species concentration data has been generated for H_2-rich low pressure flames and it was necessary to characterize these flames with respect to their H-atom profiles and temperatures.

The low pressure measurements were performed on an annular burner (inner flame diameter = 2.6 cm, overall flame diameter = 4.5 cm) contained in a vacuum housing; both burner sections are supplied with $H_2/O_2/N_2$ mixtures at flow rates of ≈30 ml(STP) s^{-1} per cm^2 of burner area. The resulting flames are stable in the pressure range 50–150 torr. As in previous work, potassium salts are supplied to the inner flame with an aspirator in the N_2 line. The aspirator is operated at or near 1 atom, which pressure is

maintained by a critical flow orifice located in the burner feed line. The boron additive compounds are added either from a hypodermic infusion pump or from the aspirator as a co-solution with the potassium salt.

A convenient operating pressure for these flames was found to be about 100 torr. Such a pressure is high enough to make diffusional ion transport unimportant* relative to convection and low enough to provide the spatial resolution necessary to obtain precise concentration profiles. With 0.1 molar solutions of KNO_3 and H_3BO_3 in the aspirator, flames are obtained at 100 torr containing total potassium and boron concentrations ($[K]_c$ and $[B]_c$, respectively) $\approx 5 \times 10^{11}$ ml^{-1}. A small ($< 1\%$, but unmeasured) amount of hydrocarbon is added to accelerate ion formation. Electron concentration measurements are performed using a large microwave resonant cavity [7] especially constructed to accommodate the low pressure burner system. Cavity data, taken in the down-stream regions of the flame where axial electron concentration gradients are small, serve as a calibration for electrostatic probe determinations [8] which, in turn, provide highly spatially resolved measurements of overall charged species concentrations.

Ion identification and changes in relative ion concentrations with reaction time are monitored mass spectrometrically. The ion mass spectrometer is used in the same configuration [3] as in previous studies.

* Based on observed profiles for BO_2^- and Cl^- in a 100 torr flame, axial diffusion velocities for negative ions are about 1 cm s^{-1} compared to a convective flow velocity of 1500 cm s^{-1}; radial profiles have not been taken but in the first 8 cm or so of flow where attachment occurs, radial diffusion may quite safely be ignored.

The only modification necessary is enlargement of the sampling orifice size when 100 torr flames are sampled. At 1 atm the sampling cone is pierced by a 0.05 mm diameter hole; at 100 torr, a cone with a 0.125 mm diameter orifice is used. The axial burner-to-sampling orifice distance is continuously variable from 0 to 25 cm.

Flame temperatures at 100 torr are measured via the conventional Na-D line reversal method. The results for the flames selected for use in this study are given in table 1 together with H-atom data at a number of positions in the flame. Temperatures were measured only in a region 6–10 cm downstream of the burner to avoid errors arising from chemi-excitation or nonequilibrium energy transfer processes in the flame front.

The H-atom concentrations in table 1 were derived from mass spectrometric measurements of the relative concentrations of $HMoO_4^-$ and MoO_3^- produced upon the addition of small quantities ($\leqslant 10^{-8}$ mole fraction) of molybdenum salts from the aspirator feed system. These two ionic species are linked through the reaction [4]

$$H + HMoO_4^- = MoO_3^- + H_2O \qquad (2)$$

for which the equilibrium constant is given by the expression $K_2 = 0.85 \exp(10400/T)$. Ion–molecule reactions of this type are sufficiently rapid to be in equilibrium at all points in the test flames and thus the ion current ratios are a good indication of the local $[H]/[H_2O]$ ratio. The values for this ratio are then used together with the equilibrium** H_2O con-

** All thermodynamic data for equilibrium calculations are taken from ref. [9].

Table 1
Low pressure (100 torr) flame characteristics

$H_2/O_2/N_2$ unburned mole ratios	T(K)	Velocity (m s^{-1})	[H] (10^{15} ml^{-1}) distance from burner (cm)						
			2	4	6	8	10	12	14
2.5:1.0:2.0	2100	11.6	12.5	12.5	12.5	12.0	11.4	11.0	10.8
2.5:1.0:3.0	1980	11.2	11.5	11.0	10.8	10.5	10.3	10.0	9.6
3.4:1.0:2.0	1830	12.1	12.0	11.4	10.7	10.3	9.8	9.4	9.0
3.5:1.0:3.0	1730	11.7	11.1	10.1	9.6	9.2	8.8	8.5	8.2

centration to compute [H]. Even though nonequilibrium effects lower the actual $[H_2O]$ to slightly below the equilibrium value, the error involved is small since H_2O is present in such relatively large quantities.

As a check on the validity of the H-atom profiles, optical absorption spectrometry was used to measure [OH]. The reaction

$$H_2 + OH \rightarrow H + H_2O \qquad (3)$$

is known to be very close to equilibrium in flames of this sort and thus a profile of relative [H] can be constructed from measurements of relative [OH] and well-established equilibrium constant for reaction (3). No attempt was made in these determinations to establish absolute values for [H]; the measurements instead serve as a check on the mass spectrometric method above. In all cases, the H-atom decay curves arrived at via both methods are in quite good agreement and the mass spectrometrically derived numbers were adopted for use in the kinetic calculations.

3. Results and discussion

Examples of the data used for the derivation of the rate constant of reaction (1) are given in figs. 1 and 2 taken at 100 and 760 torr, respectively. It may be noted that in both cases the electron and H-atom concentration curves are given in absolute units but that the $[BO_2^-]$ curve is expressed in realtive terms as ion current. This is due to the difficulties associated with absolute calibration of the mass spectrometer. Therefore, in applying the data to calculations of the rate coefficient, the mass spectrometer sensitivity appears as an additional unknown.

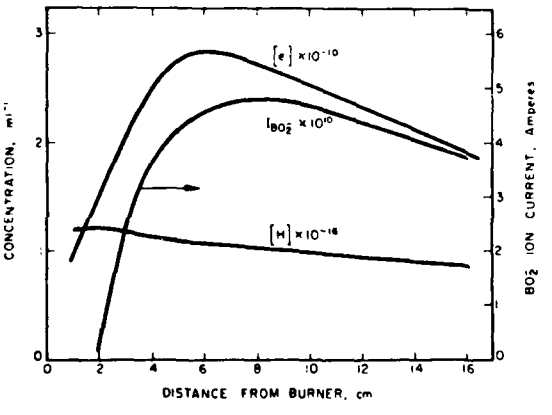

Fig. 1. Concentration profiles in 1980 K ($H_2/O_2/N_2$ = 2.5/1.0/3.0) 100 torr flame. $[HBO_2] = 7 \times 10^{10}$ ml^{-1}; velocity = 11.25 m s^{-1}.

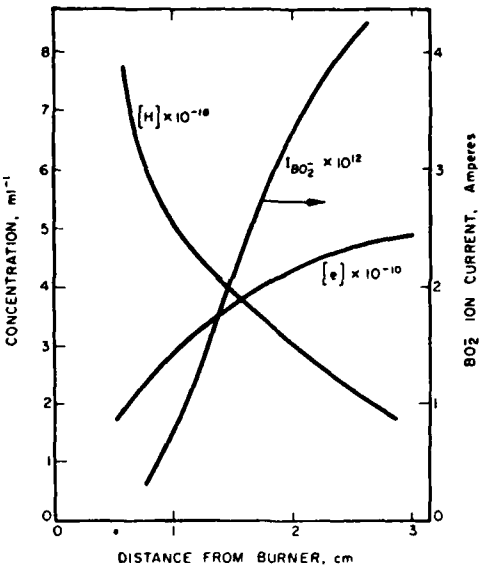

Fig. 2. Concentration profiles in 2250 K ($H_2/O_2/N_2$ = 3.5/1.0/3.0) 1 atm flame. $[HBO_2] = 3 \times 10^{11}$ ml^{-1}; velocity = 41.6 m s^{-1}.

It is also necessary in deriving an expression for the attachment rate constant to include the effects of the reverse of reaction (1). Assuming that the only source of BO_2^- is the direct attachment

$$e + HBO_2 \rightarrow BO_2^- + H \qquad (1)$$

yields the following expression for the formation of BO_2^-:

$$d[BO_2^-]/dt = k_1[e][HBO_2] - k_{-1}[BO_2^-][H] . \qquad (4)$$

By further assuming that $K_1 = k_1/k_{-1}$, where K_1 [= 1500 exp(−10000/T)] is the equilibrium constant for the reaction and inserting $I^- S$ for $[BO_2^-]$ where I^- is the BO_2^- ion current (amperes) and S is the mass spectrometer sensitivity (molecules ml^{-1} ampere^{-1}) one may derive the following equation of k_1:

$$k_1 = \frac{d(I^- S)}{dt}\left[[e][HBO_2] - \frac{(I^- S)[H]}{K_1}\right]^{-1} . \qquad (5)$$

Now, by inserting experimental numerical values of [H], [e], $[HBO_2] = [B]_c$ and $d(I^-S)/dt$ from plots such as figs. 1 and 2 at various points along the flow stream, a number of simultaneous equations for k_1 and (I^-S) are derived. Pairs of these equations are then solved for the two unknowns and the results examined for consistency. If the calculations yield constant values for both variables over the entire range of measurement, it is assumed that the mass spectrometer sampling system through-put did not change during the course of the experiment and that the rate constant data is therefore valid; it is then averaged with other results for k_1. The rate constants obtained from all seven test flames are given in table 2 together with the flame temperatures and pressures. Each of the k_1 values represents the average of several (3–5) determinations at varying concentrations (mole fractions between 10^{-9} and 10^{-6}) of alkali metal and total boron.

A plot of the bimolecular rate constant data (k_1) versus T^{-1} is given in fig. 3. The straight line drawn through the points is a least-squares line, the slope of which yields an activation energy of about 92 kJ. The Arrhenius expression for k_1 then becomes

$$k_1 = 3.2 \times 10^{-10} \exp(-11000/T)$$

$$\text{ml molecule}^{-1}\,\text{s}^{-1} . \qquad (6)$$

Since reaction (1) is endothermic by 78 kJ at 0 K, the value 92 kJ appears to be a quite reasonable activation energy.

The possible importance of three-body attachment via the reaction

Table 2
Average rate coefficients for $e + HBO_2 \rightarrow BO_2^- + H$

P(torr)	$H_2/O_2/N_2$ unburned	T(K)	k_{12}(ml molecule^{-1} s^{-1})
100	3.5/1.0/3.0	1730	8.6(−13) [a]
100	3.4/1.0/2.0	1830	7.0(−13)
100	2.5/1.0/3.0	1980	1.1(−12)
100	2.5/1.0/2.0	2100	2.8(−12)
760	3.5/1.0/6.0	1815	1.0(−12)
760	4.0/1.0/4.0	2020	1.2(−12)
760	3.5/1.0/3.0	2250	2.0(−12)

a) $8.6(-13) = 8.6 \times 10^{-13}$.

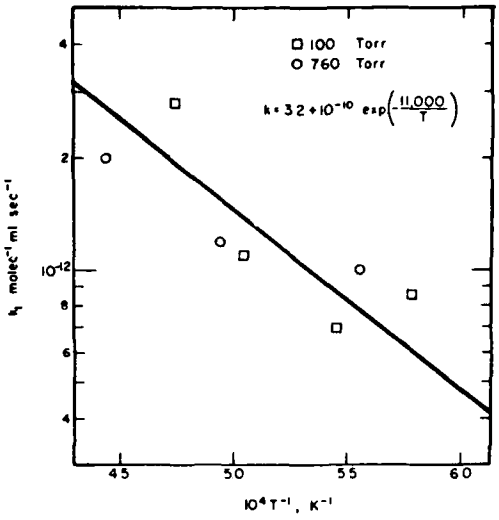

Fig. 3. Arrhenius plot for $e + HBO_2 \rightarrow BO_2^- + H$.

$$e + BO_2 + M \rightarrow BO_2^- + M \qquad (7)$$

can be assessed by comparing the relative magnitudes of the ion formation rates in the early stages of the flames where the reverse of reactions (1) and (7) are least important and the negative terms in the kinetic expressions can be ignored. If the three-body process is to have a significant effect on the overall negative ion formation process, it must be comparable in magnitude to the dissociative attachment rate; thus

$$k_1\,[e]\,[HBO_2] \leqslant k_7\,[BO_2]\,[e]\,[M] . \qquad (8)$$

By making the reasonable assumption that the reaction

$$H + HBO_2 \rightarrow H_2 + BO_2 \qquad (9)$$

is balanced (i.e., is in equilibrium) throughout the burned gases where the attachment rates were determined, eq. (8) can be rewritten

$$k_1\,[H_2]/K_9\,[H]\,[M] \leqslant k_7 , \qquad (10)$$

where K_9 is the equilibrium constant for reaction (9). Limiting values of the three-body attachment coefficient, k_7, calculated for eq. (10) are given in table 3. It can be seen from this data that if reaction (7) is to be important in the flames of this study, its rate coefficient must be very large – a factor of about 10^3 greater, for example, than either the measured values [10,11] for

Table 3
Lower limiting values for trial three-body rate contants ($cm^6\ s^{-1}$)

$H_2/O_2/N_2$ unburned	T(K)	k_7	k/T	$k/T^{1.5}$	k/T^2
3.5/1.0/3.0	1730	6.8(−27)	3.688(−30)	8.866(−32)	2.132(−33)
3.4/1.0/2.0	1830	4.3(−27)	2.374(−30)	5.550(−32)	1.297(−33)
2.5/1.0/3.0	1980	1.9(−27)	9.404(−31)	2.113(−32)	4.750(−34)
2.5/1.0/2.0	2100	4.2(−27)	2.016(−30)	4.400(−30)	9.600(−34)
3.5/1.0/6.0	1815	6.4(−27)	3.501(−30)	8.219(−32)	1.929(−33)
4.0/1.0/4.0	2020	2.7(−27)	1.309(−30)	2.913(−32)	6.482(−34)
3.5/1.0/3.0	2250	1.2(−27)	5.938(−31)	1.252(−32)	2.639(−34)

$$e + O_2 + O_2 \rightarrow O_2^- + O_2 \qquad (11)$$

or the calculated [12] upper limit for this reaction. The few determinations of three-body attachment rates currently available [13] typically lie in the 10^{-29}–10^{-30} $cm^6\ s^{-1}$ range with an inverse temperature dependence – again at variance with any of the three-body rate constants in table 3. Moreover, the data of table 3 exhibits scatter over nearly a factor of ten and no systematic variation with temperature is apparent over the range T^0 to T^{-2}. It is therefore considered quite safe to assume that the operative electron attachment mechanism in these flames is the dissociative attachment, reaction (1), and that the three-body process, reaction (7), is unimportant.

Acknowledgement

The authors wish to acknowledge the financial support for this work provided by the Office of Naval Research, Power Branch, under Contract N00014-74-C-0326 and by the Space and Missile Systems Organization (SAMSO), Air Force Systems Command, Deputy for Reentry Systems, under Contract F04701-72-C-0079.

References

[1] D.E. Jensen, Trans. Faraday Soc. 65 (1969) 2123.
[2] D.E. Jensen, J. Chem. Phys. 52 (1970) 3305.
[3] W.J. Miller, J. Chem. Phys. 57 (1972) 2354.
[4] D.E. Jensen and W.J. Miller, Thirteenth Symposium (International) on Combustion (The Combustion Institute, Pittsburgh, 1971) p. 363.
[5] D.E. Jensen and W.J. Miller, J. Chem. Phys. 53 (1970) 3287.
[6] D.E. Jensen, J. Chem. Phys. 51 (1969) 4674.
[7] P.J. Padley and T.M. Sugden, Eighth Symposium (International) on Combustion (Williams and Wilkins, Baltimore, 1962) p. 134.
[8] H.F. Calcote, Eighth Symposium (International) on Combustion (Williams and Wilkins, Baltimore, 1962) p. 622.
[9] JANAF Thermochemical Data, Dow Chemical Co., Midland, Michigian.
[10] L.M. Chanin, A.V. Phelps and M.A. Biondi, Phys. Rev. A128 (1962) 219.
[11] J.L. Pack and A.V. Phelps, J. Chem. Phys. 44 (1966) 1870.
[12] A. Herzenberg, J. Chem. Phys. 51 (1969) 4942.
[13] M.H. Bortner and T. Baurer, eds., DASA Reaction Rate Handbook, ch. 17.2.

ELECTRON ATTACHMENT KINETICS IN FLAMES: I. DISSOCIATIVE ATTACHMENT TO HCl*

William J. Miller and Robert K. Gould

AeroChem Research Laboratories, Inc.
Princeton, New Jersey 08540

ABSTRACT

This work comprises the first direct determination of the kinetics of Cl^- formation in flames. The experiments involve mass spectrometric measurements of negative ion concentrations as functions of flow time in the burned gases of well-characterized laboratory test flames seeded with small quantities of potassium and chlorine compounds. The results are consistent with the two-body dissociative attachment mechanism

$$e + HCl \rightarrow Cl^- + H$$

with a rate coefficient well represented by the Arrhenius expression

$$k = 3 \times 10^{-10} \exp(-13000/T) \text{ ml molecule}^{-1} \text{ sec}^{-1}$$

over the temperature range 1730 K to 2475 K. The flames are operated at pressures of 100 and 760 Torr. Electron concentrations were measured using a microwave resonance cavity method and positive ion profiles (total charged species) were determined with electrostatic probes. H-atom concentration profiles required to take account of the reverse detachment process are well known for the 760 Torr flames; in the low pressure flames they were obtained using a mass spectrometric negative ion tracer technique involving the known ion-molecule chemistry of molybdenum additives and confirmed via optical absorption measurements of [OH]. Contributions to Cl^- formation from three-body attachment processes are not observed. The measured values of k are found to be somewhat lower than, but in general agreement with, those inferred from electron beam and swarm studies but are much lower than the values previously derived from measurements of the reverse reaction rate.

---

† Prepared for submission to J. Chem. Phys.

INTRODUCTION

Although the reaction

$$e + HCl \rightarrow Cl^- + H \qquad (1)$$

represents the most important sink for electrons in a great many combustion systems and plasma devices, no direct measurements of its rate coefficient have yet been reported. Electron beam[1,2] and swarm[3] technique cross section measurements indicate that the rate constant is approximately given by $k_1 = 10^{-10} \exp(1 \times 10^4/T)$ ml molecule^{-1} sec^{-1}. The rate coefficient of the reverse reaction has been measured[4] near room temperature in a flowing afterglow to be 1.0×10^{-9} ml molecule^{-1} sec^{-1}. Another determination,[5] made by rapidly expanding flame gases heavily seeded with chlorine and mass spectrometrically monitoring the decrease in $[Cl^-]$ as the expanding gases cool, gives a rate coefficient for the reverse reaction similar to that obtained in the flowing afterglow. If the temperature dependence of the rate coefficient of the reverse of Reaction 1 (k_{-1}) is assumed to be small, one is led to expect, by taking the product of k_{-1} and the equilibrium constant for the reaction, that, at 2000 K, for example, $k_1 = 5 \times 10^{-9}$ ml molecule^{-1} sec^{-1}. This value, in turn, assuming the endothermicity of the reaction to be equal to its activation energy, leads to an Arrhenius expression $k = 5 \times 10^{-7} \exp(1 \times 10^4/T)$ ml molecule^{-1} sec^{-1}. This > 10-fold discrepancy in the pre-exponential factor presents a considerable problem to those who may wish to include this reaction in kinetic models of high temperature systems containing electrons, chlorine and hydrogen.

In an attempt to resolve this ambiguity, direct measurements of the rate of Reaction (1) were undertaken in a series of fuel-rich, premixed $H_2/O_2/N_2$ flames spanning a temperature range of 1730 to 2475 K. Flames burning at

760 and 100 Torr seeded with trace amounts of K and Cl were utilized. These flames provide a rapidly moving stream of hot gases containing HCl in which electron concentrations rapidly increase as K is thermally ionized. From the determination of the difference between $[Cl^-]$ and its equilibrium concentration the rate coefficient is obtained. The results yield values for k_1 similar to those inferred from the work of Refs. 1-3.

EXPERIMENTAL

The flames used in these experiments are produced on annular Meker-type burners which provide an inner flame to which additives may be supplied, surrounded by an outer identical sheath flame. The 760 Torr flames are the same as those employed in the first study of this series[6]; they have also been extensively used in thermochemical investigations and their detailed characteristics are now well known.[7-9] The 100 Torr flames have an inner flame diameter of 2.6 cm and an overall diameter of 4.5 cm. The low pressure burner is contained in a vacuum housing and is supplied with $H_2/O_2/N_2$ mixtures at rates of about 30 ml(STP)sec^{-1} per cm^2 of burner area. Chlorine and potassium are supplied to both types of flames by aspirating solutions of KCl or NH_4Cl/KNO_3 mixtures into the N_2 feed line for the inner flame.

The temperatures of the 760 Torr flames have already been well established; those of the 100 Torr flames were measured using the conventional Na-D line reversal method. Electron concentrations were measured using microwave cavities[10] which were, in turn, used to calibrate electrostatic probe measurements of the positive ion concentration.[11] The probe measurements provide highly spatially resolved measurements of the positive ion concentration (and hence of the electron concentration since negative ion concentrations are in all cases relatively negligible in these experiments). H-atom profiles are

well known for the 760 Torr flames; for the 100 Torr flames, they were determined in two ways. First a mass spectrometric measurement of the ratio of $[HMoO_4^-]$ and $[MoO_3^-]$ was made along the axis of the flames seeded with traces ($\leq 10^{-8}$ mole fraction) of molybdenum salt. These ionic species are linked through the reaction[8]

$$H + HMoO_4^- \rightleftarrows MoO_3^- + H_2O \qquad (2)$$

which is known to be balanced in the 760 Torr flames. Secondly, optical absorption measurements were made to determine profiles of [OH]. This concentration can then be related to relative [H] by noting that the reaction

$$OH + H_2 \rightleftarrows H_2O + H \qquad (3)$$

is very nearly balanced in flames of this type. Since only relative [H] profiles were obtained in the latter measurements, these serve only as a check on the mass spectrometric absolute concentration profile measurements. In all cases the shapes of the profile curves obtained using the two methods were similar and the mass spectrometrically obtained values of [H] were used in the kinetic calculations.

The electron, positive ion or negative ion axial profile measurements were obtained by raising and lowering the burner relative to the appropriate measuring device; in the case of the 760 Torr flames the flames were examined between 0.2 cm and 5 cm from the burner. In the case of the 100 Torr flames, scans were made over a range of 2 to 14 cm above the burner. In Table I the principal flame parameters along with the H-atom profiles measured here and in earlier work are given.

RESULTS AND DISCUSSION

If it is assumed that the variation of $[Cl^-]$ is controlled solely by Reaction (1) and its reverse, i.e., that 3-body attachment is not important and that radial and axial diffusion are not important, then the rate of change in $[Cl^-]$ along the axis of the flame is simply given by

$$\frac{Cl}{dt}[Cl^-] = k_1[e][HCl] - k_{-1}[Cl^-][H] \qquad (4)$$

Assuming that $K_1 = k_1/k_{-1}$ where K_1 is the equilibrium constant for Reaction (1) and letting S be the mass spectrometer sensitivity, then Eq. (4) may be written in terms of the mass spectrometer Cl^- ion current, I^-, and rearranged to give

$$k_1 = v_f \frac{d}{dz}(I^-S) \left\{ [e][HCl] - \frac{(I^-S)[H]}{K_1} \right\}^{-1} \qquad (5)$$

where v_f is the velocity of the burned gases and z is the height above the burner.

Equation (5) may be solved for k_1 directly by taking the slopes of the measured I^- profiles along with values of [e] and [H] at pairs of points along the I^- profiles and then eliminating S from the pairs of equations. This method has proved to yield reproducible (within a factor of about 3) results from data taken over a period of several weeks while obviating the necessity of making an absolute calibration of the mass spectrometer. This last is an important consideration, since, because of kinetic effects which may be present in any 'calibration flame' in which a source of negative ions is present, (i) there is no straightforward method of calibrating the flame ion mass spectrometer for negative ions to much better than a factor of 2 and (ii) from an experimental point of view, the calibration factor is different for each flame and subject to drift from day to day.

From each I^- curve three pairs of points were typically selected and values for k_1 obtained. In most cases these values for k_1 were in good agreement with one another. Since slight shifts in (i) the rate at which CsCl was supplied to the flame, (ii) throughput of flame gases to the mass spectrometer or (iii) mass spectrometer sensitivity all may occur during a run, large deviations occasionally occurred in the set of values for k_1 from a single ion profile, in which case the runs were repeated. Figure 1 is an Arrhenius plot of the average values of k_1 found for each flame. Each point represents the average of values obtained from four to six ion profiles. The experimental uncertainty in each point is $\approx \stackrel{\times}{\div} 3$. The least squares line fitted to the data gives

$$k_1 = 3 \times 10^{-10} \exp(-13100/T) \text{ ml molecule}^{-1} \text{ sec}^{-1} \qquad (6)$$

The question of the validity of the simplifying assumption used in writing Eq. (4) may be answered in part by the following arguments. With regard to diffusion, rough calculations show axial diffusion to have a very small effect on the axial distribution of species in the flame. A 'diffusion velocity', v_d may be defined by

$$v_d = - \frac{D}{[Cl^-]} \frac{d[Cl^-]}{dz} \qquad (7)$$

where D is the ambipolar diffusion constant of Cl^-. The maximum value of $[Cl^-]^{-1}(d[Cl^-]/dz)$ observed is ≈ 2 cm^{-1}. D_{Cl^-} in these flames may be estimated to be ≈ 10 cm^2 sec^{-1} ($D_{H_3O^+} \approx 12$ cm^2 sec^{-1} in flames such as these[10]). Thus the ratio $v_d/v_f \gtrsim 0.02$, i.e., axial diffusion would require no more than 2% correction to the data. Similar considerations lead to similar results with regard to radial diffusion.

The possibility that the reaction

$$e + Cl + M \rightarrow Cl^- + M$$

may be competing with Reaction (1) should be considered. The ratio of the rate of Reaction (8) to that of Reaction (1) would be given by the expression

$$\frac{k_8}{k_1}\frac{[Cl][M]}{[HCl]} \approx \frac{k_8}{k_1} K_{10} \frac{[H][M]}{[H_2]} \qquad (9)$$

where K_{10} is the equilibrium constant for the reaction

$$H + HCl \rightleftarrows H_2 + Cl \qquad (10)$$

which, because of the large concentration of H and H_2, must be nearly balanced throughout the burned gas region of the flames. Values for $K_{10}[H][M]H_2]^{-1}$ (in order of decreasing magnitude) are listed in Table II. From this data it may be seen that the contribution to the rate of production of Cl^- from Reaction (8) would be greatest in the 760 Torr, 2475 K and 2250 K flames and the 100 Torr, 1980 K flame. These flames, then, should yield anomalously high values for k_1 relative to the other flames if Reaction (8) was important. The two flames which gave values of k_1 furthest from the least squares line in Fig. 1 are the 760 Torr, 2250 K flame (low) and the 760 Torr, 1818 K flame (high). This is opposite to what would be expected if Reaction (8) were contributing to Cl^- formation. In fact, the data of Fig. 1 show no tendency at all to be sensitive to the parameter in the right hand column of Table II. Thus the data appear to argue against Reaction (8) being a significant process.

Recent cross section measurements[3,12] for Reaction (1) show that the peak cross section occurs at 81 kJ $mole^{-1}$ (9.84 eV). On the basis of these determinations the activation energy for Reaction (1) measured here (109 kJ $mole^{-1}$) appears too large. However, it may be seen from the dashed line in Fig. 1 which corresponds to an expression for k_1, with an activation energy of

81 kJ mole^{-1} that this temperature dependence falls well within the limits of error imposed by the scatter in our data. If 81 kJ mole^{-1} is the actual activation energy, the expression for k_1 becomes

$$k_1 = 5 \times 10^{-11} \exp\left(\frac{-9750}{T}\right) \text{ ml molecule}^{-1} \text{ sec}^{-1} \qquad (11)$$

The comparison of the rate coefficient measured here with values inferred from electron beam and swarm experiments requires evaluation of the following integral

$$k = \frac{2^{3/2}}{(\pi m k^3 T^3)^{1/2}} \int_0^\infty Q\, E \exp\left(-\frac{E}{kT}\right) dE \qquad (12)$$

Where Q is the cross-section, m the reduced mass (approx. the mass of the electron) and E the center-of-mass kinetic energy. The shape of the cross-section vs. energy curve peaks sharply at E_o = 0.84 eV.[3,12] The width of the cross-section is not known, but one would expect onset to be near 0.82 eV, the value of the difference between dissociation energy of HCl and the electron affinity of Cl.[13] The assumption that the cross section can be represented by a Gaussian

$$Q = Q_o \exp\left(-\frac{(E-E_o)^2}{2\sigma^2}\right)$$

where σ = 0.02 eV leads to the following estimation of k_1 at 2000 K

$$k_1 \approx \frac{4E_o\sigma\, Q_o}{m^{1/2}\,(k^3T^3)^{1/2}} \exp\left(-\frac{E_o}{kT}\right) = 4\times10^7\, Q_o \exp\left(-\frac{9750}{T}\right) \text{ ml molecule}^{-1} \text{ sec}^{-1} \qquad (13)$$

If Q_o is taken to be 4×10^{-18} cm^2 or 2×10^{-17} cm^2, the low[1] and high[3] values for the measured peak cross section, pre-exponentials of 8×10^{-10} and 1.6×10^{-10}, respectively, are obtained in Eq. (13). Thus the

present measurement appears to favor somewhat the former, lower value, being at 2000 K about a factor of 3 below that inferred from Ref. 1.

Regardless of which of the above expressions for k_1 is adopted, a considerable discrepancy exists between these direct high energy (temperature) measurements of the rate of Reaction (1) and the values derived via the equilibrium constant and measurements of the rate coefficient for the reverse associative detachment. For example, the measurements of Burdett and Hayhurst[5] and Howard et al[4] of k_{-1} at lower temperatures lead to values of the pre-exponential for k_1 of 4×10^{-7} to 2×10^{-6} when extrapolated to 2500 K. As noted in Ref. 5, these values indicate, in turn, peak cross sections for Reaction (1) on the order of 10^{-14} cm^2 or larger--some 10^3 to 10^4 times greater than those of the present work or of Refs. 1-3. We can offer no explanation for this discrepancy at this time other than marked changes in the detailed reaction mechanism with temperature or a temperature dependence for the pre-exponential of k_1 such as T^{-3}. These questions are likely to be resolved only by direct measurements of k_1 at intermediate temperatures.

REFERENCES

* Support for this work was provided by the Office of Naval Research, Power Branch, under Contract N00014-74-C-0326

1. I.S. Buchel'nikova, Sov. Phys. JETP 35, 783 (1959).
2. R. Azria, L. Roussier, R. Paineau, and M. Tronc, Rev. Phys. Appl. 9, 469 (1974).
3. L.G. Christophorou, R.N. Comption, and H.W. Dickson, J. Chem. Phys. 48, 1949 (1968).
4. C.J. Howard, F.C. Fehsenfeld, and M. McFarland, J. Chem. Phys. 60, 5086 (1974).

5. N.A. Burdett, A.N. Hayhurst, Nature Phys. Sci. 245, 77 (1973).

6. W.J. Miller and R.K. Gould, Chem. Phys. Lett. (in press).

7. D.E. Jensen, Trans. Faraday Soc. 65, 2123 (1969).

8. D.E. Jensen and W.J. Miller, Thirteenth Symposium (International) on Combustion (The Combustion Institute, Pittsburgh, 1971), p. 363.

9. D.E. Jensen and W.J. Miller, J. Chem. Phys. 53, 3287 (1970).

10. P.J. Padley and T.M. Sugden, Eighth Symposium (International) on Combustion (Williams and Wilkins, Baltimore, 1962), p. 134.

11. H.F. Calcote, Eighth Symposium (International) on Combustion (Williams and Wilkins, Baltimore, 1962), p. 622.

12. J.P. Ziesel, I. Nenner, and G.J. Schulz, J. Chem. Phys. 63, 1943 (1975).

13, JANNAF Tables, Dow Chemical Co., Midland, MI.

TABLE I. FLAME CHARACTERISTICS

$H_2/O_2/N_2$ (unburned mole ratios)	T, K	Velocity (m sec^{-1})	[H], 10^{15} ml^{-1} (distance from burner, cm)						
760 Torr Flames					1	2	3	4	5
3.4/1.0/2.0	2475	45.5			55	43	39	36	34
3.5/1.0/3.0	2250	41.6			43	27.8	20.8	17.6	13.7
4.0/1.0/4.0	2020	26.3			27.4	15.8	11.1	8.6	7.0
3.5/1.0/6.0	1815	13.1			9.8	5.9	4.2	3.3	2.7
100 Torr Flames			2	4	6	8	10	12	14
2.5/1.0/3.0	1980	11.2	11.5	11.0	10.8	10.5	10.3	10.0	9.6
3.4/1.0/2.0	1830	12.1	12.0	11.4	10.7	10.3	9.8	9.4	9.0
3.5/1.0/3.0	1730	12.7	11.1	10.1	9.6	9.2	8.8	8.5	8.2

TABLE II

VALUES FOR $K_{10} \frac{[H][M]}{[H_2]}$ IN THE TEST FLAMES

P, Torr	T, K	K_{10}	$K_{10} \frac{[H][M]}{[H_2]}$, ml^{-1}
760[a]	2475	0.704	1.6×10^{17}
760	2250	0.719	1.6×10^{17}
100[a]	1980	0.742	1.1×10^{17}
760	2020	0.738	9.7×10^{16}
100	1730	0.770	5.4×10^{16}
760	1815	0.759	4.6×10^{16}
100	1830	0.757	3.7×10^{16}

[a] Distance above the burner is 1 cm for 760 Torr flames, 2 cm for 100 Torr flames.

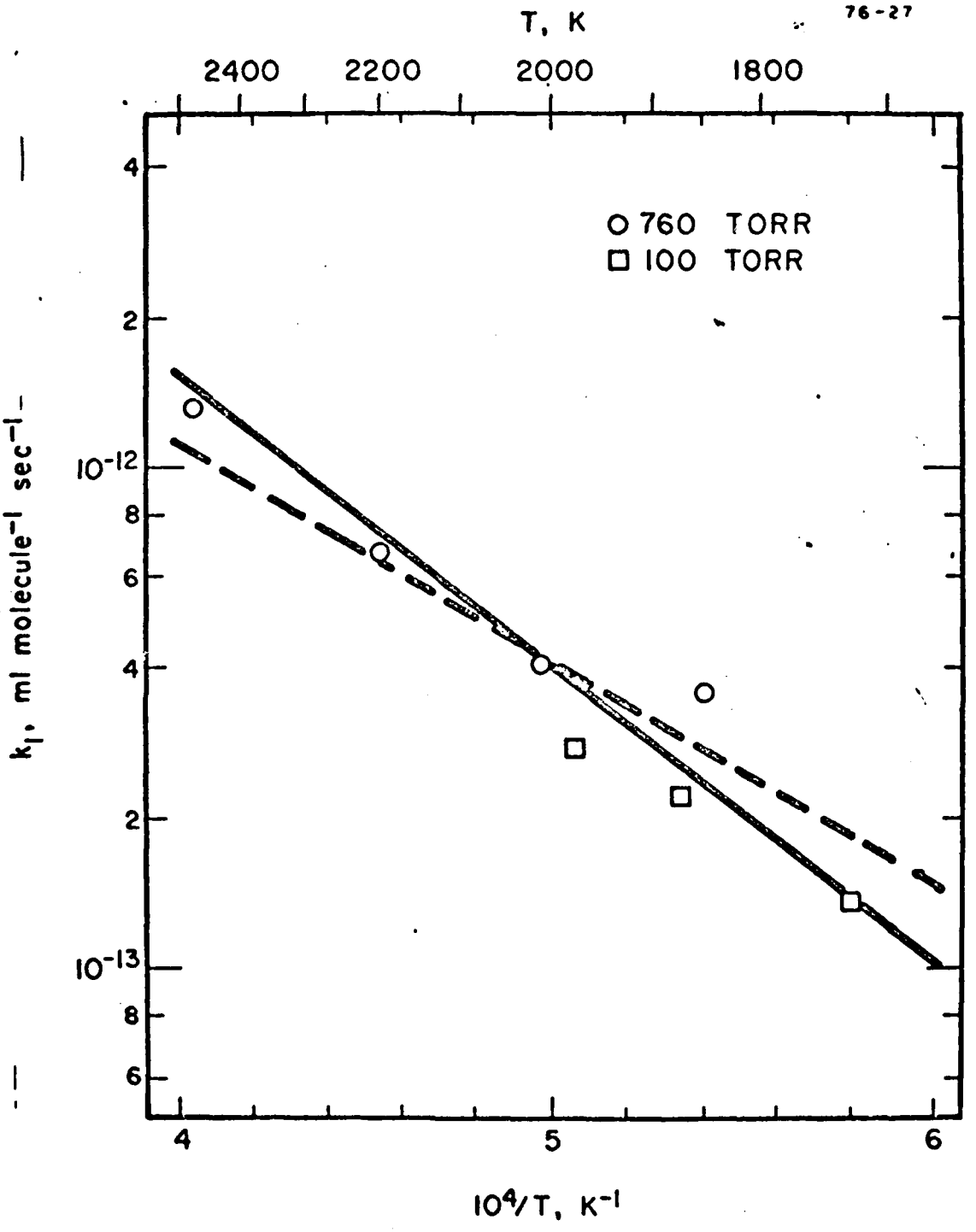

Fig. 1 Average values for the dissociative attachment rate coefficient obtained in the seven test flames. The solid line is a least-squares fit to the data representing $k_1 = 3 \times 10^{-10} \exp(-13100/T)$. The dashed line has a slope of 81 kJ mole^{-1}, the activation energy expected from the work of Refs. 3 and 12.

APPENDIX C

AeroChem TP-331 NOVEMBER 1975

CHARGED SPECIES DIAGNOSTICS FOR COMBUSTION SYSTEMS

William J. Miller *
AeroChem Research Laboratories, Inc.
P.O. Box 12, Princeton, New Jersey 08540

ABSTRACT

This paper describes briefly a number of plasma diagnostic techniques which have been widely used for the measurement and characterization of charged species in combustion systems. The limits of applicability, sensitivity and accuracy of the methods are discussed and the working equations by which the experimentalist reduces data are presented. Extensive literature references are also provided in which to find detailed accounts of apparatus construction and the development of the mathematical models upon which the working equations are based. Techniques described include electrostatic probes, microwave cavity and cyclotron resonance, electromagnetic-wave attenuation and mass spectrometry.

Introduction

The ionization phenomena associated with nearly all practical combustion systems have been subjects of scientific research for well over a century. Subsequent to World War II, appreciation of the importance of ion and electron chemistry in systems such as rocket exhausts, re-entry wakes, combustion-driven MHD devices and flame ionization detectors has stimulated the development and application of a wide variety of diagnostic tools for the detection and measurement of charged species in combustion environments. The objectives of this paper are to review a number of the more commonly employed diagnostic techniques, illustrate their utility by presenting samples of experimental data and provide potential users with literature references to more detailed descriptions of their applications. The methods discussed in greatest detail are those which have proven most useful to the laboratory experimentalist as tools rather than as subjects of research in themselves. It is not the intention of this paper to present an extensive description of the theoretical development underlying various methods; that information is included only by reference to the literature. The emphasis here is on the capabilities, limitations and accuracy of a few well-used techniques, and the working equations through which the raw data obtained are converted to the desired appropriate plasma property. The discussion includes descriptions of electrostatic probes, some microwave and radiofrequency methods and mass spectrometry; the various optical techniques used for combustion plasma studies (i.e. methods employing wavelengths up to and including the far infrared) are not discussed here; the interested reader is referred to the spectroscopic literature (e.g. Refs.1 and 2).

Electrostatic Probes

The oldest and, still, the most commonly performed flame plasma measurements involve a determination of the current flow between two electrodes placed in or near the flame and biased at different potentials. Several kinds of information may be extracted from data obtained in this way, depending upon the magnitude of the voltage differential and the relative sizes of the probes and the combustion system. If the impressed electric field is large ($\geq$ 100 V/cm), and the probes are substantial in size (i.e. approaching the size of the flame, or larger), charged species will be drawn out of flame essentially as they are formed. Recombination is thus all but eliminated and the current measured between the electrodes is directly proportional to the ion formation rate. These measurements serve as the basis for the flame ionization detectors[3] used primarily in gas chromatography for the detection and identification of hydrocarbons. A schematic of a typical detector[4] of this kind is given in Fig. 1. It depends for its operation on the low level of ionization exhibited by H_2/air flames[5] and the fact that the combustion of non-oxidized, carbonaceous material introduced into these flames gives rise to a nearly constant fraction[6] of ions per carbon atom regardless of the chemical structure of the molecule. These systems are routinely made to respond linearly to the carbon content of the gas stream over a 10^7-fold range of sensitivity and they are thus ideally suited to the analysis of gas streams emerging from chromatography columns. The probe response, however, is simply a macroscopic measure of flame conductivity; it reveals nothing about the details of the gas dynamics or the chemistry of the flame.

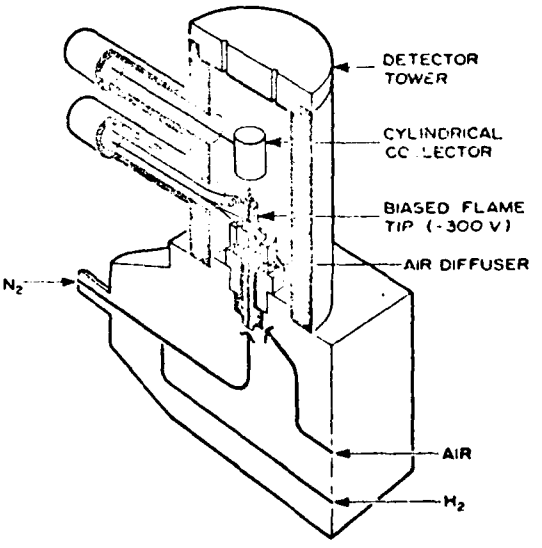

Figure 1. Cross-Sectional View of Flame Ionization Detector for Gas Chromatography. (from Ref. 4)

The use of very small probes at variable collection voltages has produced the greatest proportion of our present knowledge of the detailed plasma properties of high temperature combustion

* Head, Combustion Chemistry Group

Prepared for presentation at the 14th AIAA Aerospace Sciences Meeting, Washington, DC, January 1976, to be published in AIAA Progress in Astronautics and Rocketry Series.

systems. The current vs. voltage 'probe curves' obtained' from small cylindrical or spherical probes can, in principle, be interpreted to yield local values of charged species concentrations and electron temperatures. The probes themselves are fairly easy to build; the minimum necessary instrumentation includes only a variable d.c. voltage source and an electrometer of some sort. The data is deceptively simple to collect and, if anything, there is an overabundance of theories available with which to interpret the results.

Double probes, as the name implies, comprise two electrodes of the same size inserted into the plasma for the purpose of withdrawing charged species. Since the critical measurement is the flow per unit probe area of ions or electrons across the gaseous sheath of shifting potential surrounding the probe, it is extremely important that voltage losses from the probe through its insulation be eliminated and that the probe area be well defined. The construction of such probes for use in hostile combustion environments is not a trivial task.

Figure 2 illustrates a typical' probe of cylindrical geometry. The quartz tubing provides the insulation which is protected from dielectric degradation due to heating by the silver cooling jacket. The probe wire itself must be of a material refractory to flame constituents and capable of heating to high temperatures. It should also be non-catalytic with respect to atom and radical recombination to preclude overheating due to these effects. Platinum[8] and (preferably) platinum-rhodium alloys (e.g. see Refs. 7, 9-11) have been used successfully by a number of workers; it is wise to avoid the use of platinum, however, since it is notorious for exhibiting catalytic effects in H-containing flames. It should also be well noted that the probes, whether 'double' or 'single', must be kept as small as practicable so that the probe operation itself does not alter the plasma properties it seeks to measure; i.e. the probe should not withdraw enough charged species to change the plasma potential significantly.

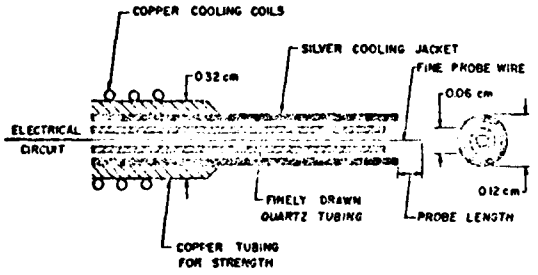

Figure 2. Electrically and Thermally Insulated Probe.

An example of a current-voltage curve from a double probe is given in Fig. 3. It can be seen from this data that the 'saturation' currents at high potentials drawn by the two probes are nearly equal and that the curve is nearly symmetrical. This is due to the fact that the charged species of lowest mobility (greatest mass) controls the current flow to both probes and only its concentration may, therefore, be measured. In high temperature systems then, where the predominant negatively charged species are electrons, these curves are controlled by positive ion collection and the method is incapable of yielding electron densities. A perfectly symmetrical double probe curve, unfortunately, represents an ideal situation in which the probes are identical in size and geometry and both are surrounded by gases with identical plasma potentials. In practice (e.g. in the case illustrated by Fig. 3), this condition is difficult to achieve for a variety of reasons discussed in detail in Ref. 9. Despite these difficulties, double probe methods have been widely and successfully employed to measure positive ion concentrations and, from the nature of the curve in the rapidly changing portion at small probe voltage differences, electron temperatures. The means by which the data is interpreted in both these cases, however, is identical, in essence, to that employed for single probes and they can be conveniently discussed jointly.

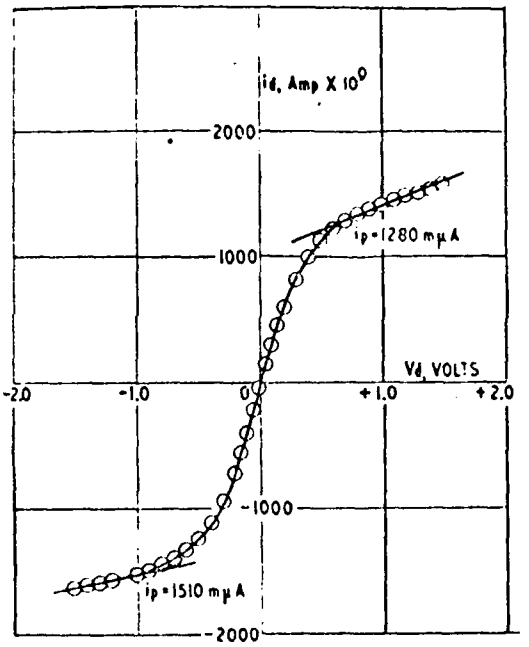

Figure 3. Double Probe Current-Voltage Characteristic (from Ref. 8).

If the size of the positively charged electrode can be increased sufficiently, saturation with respect to the electron current can be achieved and electron densities can be derived as well. This condition is attained by making the second electrode the burner and/or large screens inserted at various positions in the plasma, taking care that conditions about the small probe are not affected. The ratio of the probe areas required to achieve adequate positive ion transport when the small probe is sampling electrons has been shown[12] to be $\geq 10^3$. This is equivalent to saying that the 'single' probe must be very small. The difficulty in achieving this condition is illustrated in Fig. 4 which is a sample single probe curve of a kind unfortunately, frequently encountered; electron

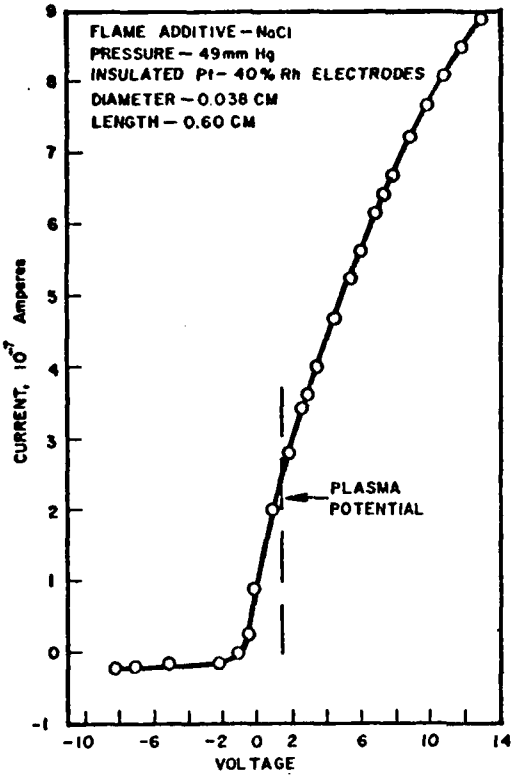

Figure 4. A Typical Single-Probe Current-Voltage Characteristic (from Ref. 9).

saturation at positive probe potentials has not been attained due to the inadequate size of the negative electrode. The large electrode in this case was a 3.8 cm diameter Meker-type burner, giving an electrode area ratio of ~ 150. An alternative technique to increase the positive ion flux, involving the addition of a third independently biased electrode, has been suggested by Yanage[13,14] but there are reservations[12] as to its effect on the bulk plasma properties. In short, although electron concentration measurements using single probes are straightforward in principle, they are very difficult in practice and great care must be exercised in order to obtain accurate results.

Many theories have so far been advanced for the interpretation of electrostatic probe curves taken under various conditions. The theories take into account, among many things, probe geometry, the magnitude of the applied potential, the effects of plasma velocity and the changes in plasma properties induced by variations in combustion system pressure. To the laboratory experimentalist this frequently represents an overabundance of models from which to choose; in fact, the differences in charged species concentrations computed using the various approaches seldom fall outside the accuracy limitations imposed by the data itself. One of the simplest and most widely used theories for the interpretation of probe data in combustion systems is that of Bohn, Burhop and Massey[15] as modified by Calcote.[16,17] This theory, for the usual case of cylindrical probes (of length L and diameter d), relates the value of the positive ion current (j_+) obtained by extrapolating the negative voltage portion of the probe curve to the plasma potential (V_p, see Fig. 4), to the positive ion concentration, N_+, through the expression

$$N_+ = j_+ \left(\frac{2\pi m_+}{k T_+ e^2} \right)^{1/2} \left\{ 1 + \frac{0.19\, Ld}{\lambda_+ B} \ln\left(\frac{X+B}{X-B} \right) \right\} \quad (1)$$

where m_+ is the positive ion molecular weight, T_+, its temperature and λ_+, its mean-free path; e is the charge of an electron, $X = L + 2\lambda_+$ and $B = \{X^2 - (d+2\lambda_+)^2\}^{1/2}$. For probes of other than cylindrical geometry, only the quantity in brackets changes form; a corresponding expression for ellipsoidal (or, in one limit, spherical) probes is given in Ref. 7. Directly analogous expressions may be written for electron concentration (N_e) determinations in which all the subscripted quantities for positive ions are replaced by their corresponding electron values.

The uncertainties inherent in the use of Eq. (1) lie in the local identification of m_+, the estimation of λ_+ and in extrapolation of the ion current curve to V_p. The latter is, of course, dependent upon proper identification of the 'break' point in the electron current vs. voltage curve which defines the plasma potential. Obviously, if saturation is not obtained, as in Fig. 4, the proper value of V_p cannot be determined. Fortunately, since the slope of the positive ion saturation curve is small, this source of error is usually negligible in measurements of positive ion concentraions. It should be noted, however, that this is true only of the positive ion current; the extent to which the probe falls short of achieving electron saturation is directly proportional to the resultant error in N_e.

Charged species transport due to convective flow is not accounted for in Eq. (1) although such effects are commonly encountered in combustion systems. Neglect of this effect can be of considerably greater import than the errors in positive ion determinations so far discussed. Jensen and Kurzius[18] have presented a modified version of Eq. (1) which includes a consideration of mass flow and is generally applicable to any laminar, high velocity, subsonic system. For the frequently encountered instance of a cylindrical probe with its axis normal to the flow, n_+ is given by

$$n_+ = j_+ \left\{ \left(\frac{2\pi m_+}{k T_+} \right)^{1/2} + \frac{d}{(Sh)\, D_\pm} \right\} \quad (2)$$

where D_+ is the ambipolar diffusivity and (Sh) is the perimeter-mean Sherwood number given, in terms of the Reynolds (Re) and Schmidt (Sc) numbers, by the expression

$$(Sh) = 0.55\, (Re)^{1/2}\, (Sc)^{1/3} - 2 \ln\{2(L + 2\lambda_+)/d + 2\lambda_+)\} \quad (3)$$

Tests of this approach have so far been limited to positive ion determinations; the validity of the analogous expression for n_e has not been investigated.

In addition to yielding electron and positive ion number densities, electrostatic probes are also used for measurements of electron temperatures. However, the proper means of performing these measurements has been the subject of considerable controversy for more than a decade. In principle, the slope of a plot of ln[electron current] vs. applied voltage is equal to e/kT_e, the electron current being the observed external probe circuit current minus the extrapolated positive ion saturation current at the applied voltage. Workers[7,19,20] using single probe curves in this fashion, however, frequently found extremely high electron temperatures in a narrow region within hydrocarbon flames while those employing double probes[8,21,23] in similar flames, usually obtained values close to the gas temperature throughout the entire flame. It is now generally accepted that the latter is true; the departures of T_e from the gas temperature in normal flames are, at most, a few hundred degrees[24,25] and they only occur very close to the flame front. The source of these discrepancies in single probe measurements are attributed to the use of data taken too far from the positive ion saturation region; when single and double probe data from the portions of the respective curves close to positive ion saturation are directly compared, as in Ref. 9, the T_e's are nearly identical. Similarly, despite the diverse assumptions underlying the various available probe theories and the supposed differences in their domains of applicability, the same conclusion is reached[26,9] using the simple theory of Calcote[7] or those of Su and Lam,[27] Lam,[28] Johnson and Malter,[29] or Cohen.[30] For the purist who wishes to analyze electrostatic probe behavior in detail, extensive discussions of the above and many other theories are conveniently brought together in Ref. 31.

Microwave Cavity Resonance

If a microwave cavity is built so as to include a plasma or a flame containing ionized species, its Q factor (defined as the ratio of energy stored/energy lost) at resonance becomes a function of the dielectric constant, and thus the electron content, of the plasma. Specifically, the technique which has proven most useful is one in which the cavity is of a geometry suitable for resonance in the TM(010) mode at a specific microwave frequency, ω, between 1 and 4 GHz. A schematic of such a cavity, together with the burner and flame system to which it is coupled, is shown in Fig. 5. In practice,[32-35] these cavities are annuli about 10 cm in diameter and a few mm high. The hole in the center can be as large as about 3 cm without seriously affecting its performance. They must, of course, be cooled to prevent thermal degradation by the flame and they should be thermostated to minimize drift due to small changes in geometry. The spatial resolution of electron concentration measurements made along the flame axis is typically about the same as the cavity height except in the region of the flame close to the burner where the Q factor of the cavity is influenced by the presence of the burner itself.

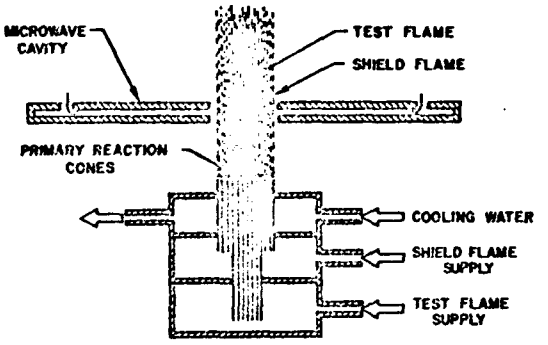

Figure 5. Burner and Microwave Cavity.

A representative circuit[32] for utilizing cavity resonance effects is given in Fig. 6. Microwave power from a tunable klystron (V_s) with a variable output impedance, R_s, is fed into the cavity through one of the antennae indicated in Fig. 5. L, C, and R_c represent, respectively, the inductance, capacitance and resistance of the cavity itself. The impedance R_L is provided by a crystal diode rectifier across which a d.c. voltage (V_L) or current flow (I) is measured. After setting up the circuit and determining the TM(010) resonant frequency in the presence of a flame containing no electrons, an ionizable material may be added to the flame to produce electrons and the characteristics of the circuit redetermined. An analysis of the electrical properties of the cavity shows that the Q of the cavity and its resonant frequency before the addition of electrons (subscript 'o') is related to that with electrons (no subscript), through the expression

$$\frac{Q_o}{Q} - 1 = \left[\left(\frac{\omega_o}{\omega}\right)^{1/2} - 1 + \frac{A\sigma Q_o}{\omega}\right] \qquad (4)$$

where A is a constant dependent on cavity geometry and σ is the conductivity of the plasma. For cavities of the sort described above, it has been shown[36] shown that the frequency shift, in reality, is small in comparison to the change in σ and the term in brackets in Eq. (4) can be neglected. Now, if $R_S R_L/(R_S + R_L) \gg R_c$, it has been further shown that $I \propto Q^2$ and, since $\sigma \propto n_e$, one may derive the following expression for the electron concentration in terms of the d.c. currents before and after their introduction (I_o and I, respectively):

$$\left(\frac{I_o}{I}\right)^{1/2} - 1 = C\, n_e \qquad (5)$$

In this equation, C is a number of combined constants and must be determined by direct calibration.

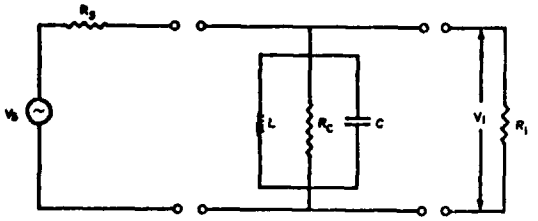

Figure 6. Equivalent Circuit of Cavity System (from Ref. 32).

To calibrate the cavity, a flame of known electron content can be used. A large number of these are now available as a result of an extensive series of investigations* using cavities and a number of other diagnostic methods as comparative cross-checks. Once a value of C has been determined from the known n_e and the observed d.c. current ratio, it is valid over the entire available range of cavity response but, strictly speaking, only for that flame used in the calibration. Since C depends on the electron-neutral collision frequency (ν_e), which is a function of gas composition and temperature, it will vary from flame to flame. This is, fortunately, not found to be a significant source of error unless the H_2O content of the flame changes appreciably; a calibration performed in H_2/O_2 flames would not, however, be expected to be adequate in flames of CO/O_2, for example.

The accuracy of this technique is as good as the calibration allows and the sensitivity is a direct function of the cavity constant. In its implementation, the method has proven useful, practically, in the range $10^9 < n_e < 10^{12}$ cm^{-3}. At the lower limit of this range, the system must be very noise-free and stable; even with well-designed cavities, at $n_e = 10^9$ cm^{-3}, one must be able to detect a change in I of a few parts per 10^3 or less. The most severe limitations on the usefulness of the method are imposed by its geometrical requirements. The plasma to be studied must be a part of the cavity and thus the overall dimensions of the apparatus must be large relative to those of the flame. Despite its applicability to rather small combustion systems of somewhat specialized configuration, this technique has proven of great value in basic laboratory combustion studies.

Cyclotron Resonance

When a flame or other plasma is intersected by a magnetic field and a microwave beam at right angles to one another, absorption of electrical energy may occur and the transmitted electrical energy is attenuated. In low pressure plasmas, in which the microwave frequency, ω, is made large with respect to the plasma frequency, ω_p, the maximum attenuation takes place at the electron cyclotron resonant frequency. The magnitude of this attenuation, and the bandwidth over which it occurs, are directly related to, and thus can be used to measure, both n_e and the electron collision frequency, ν_e.

Since the impression of a significant magnetic field on the plasma requires rather bulky apparatus, this method is also applicable primarily to small laboratory systems. The most convenient measurements have proven[40-44] to be those in which the beam frequency, ω, is fixed at a value $>> \omega_p$, the magnetic field strength, H, is swept through the resonant condition and the microwave power transmission is measured as a function of H. A plot of β, the microwave attenuation, vs. H then exhibits a peak at some field value, H_o, which, together with the measured width of the peak at half maximum, gives the electron collision frequency via Eq. (6):

$$\nu_e = \frac{\Delta H\ \omega}{2\ H_o} \qquad (6)$$

For this equation to be valid, the width of the resonance line, ΔH, must be the result of collisional broadening and this requirement is very stringent. Gray[45] has computed that, in fact, $(\omega_p/\omega)^2$ must be 'considerably below 0.1'. This restriction, in practice, limits the applicability of the method to subatmospheric pressure plasmas and flames with $n_e \leq \sim 10^{11}$ cm^{-3}.

Within the same limitations as above, the β vs. H curve yields the electron concentration through the equation[46]

$$n_e = 3.8 \times 10^7\ \beta\ \Delta H/L \qquad (7)$$

where L is the microwave path length through the (uniform) plasma. This measurement, and the ν_e determination above, when made via this technique, have the advantages that no perturbation of the plasma by a probe is necessary and that the method requires no calibration. Its accuracy, in principle, should be quite good since no absolute measurements are required other than those of ω and H, both of which can be quite precisely metered. Besides the rather limited scope of applicability, however, the method also suffers the disadvantage of poor spatial resolution ($\sim$ 0.5 cm) so that detailed flame structure determinations are difficult.

Direct Attenuation and Other Microwave Methods

Since both of the resonance methods described above involve surrounding a combustion system with a considerable amount of apparatus, the sizes of the plasmas that are accessible to study is limited, in reality, to those of laboratory test flames. The plasma properties of larger systems such as rocket exhausts must be examined through the use of rugged electrostatic probes[47,48] or through the interaction of the plasma with focused beams of electromagnetic energy, specifically, microwaves. When a microwave beam encounters a plasma, it can be measurably attenuated, refracted or reflected, depending on the local values of n_e, ν_e and ω.

* The series includes work by a number of workers and is, in fact so extensive that it is impractical to list them here. The interested reader is referred to reviews of the subject, e.g. Refs. 37-39.

Attenuation measurements must be made under the conditions $\omega >> \omega_p$; if, in addition, $\omega \gtrsim \nu_e$ the attenuation, β, in dB/cm path length is given by

$$\beta = 0.46 \frac{n_e \nu_e}{\nu_e^2 + \omega^2} \quad (8)$$

Values of n_e and ν_e can, therefore, both be obtained from a determination of attenuation at two or more different frequencies. A schematic of a typical apparatus for measuring attenuation in a rocket exhaust flame is shown[49] in Fig. 7.

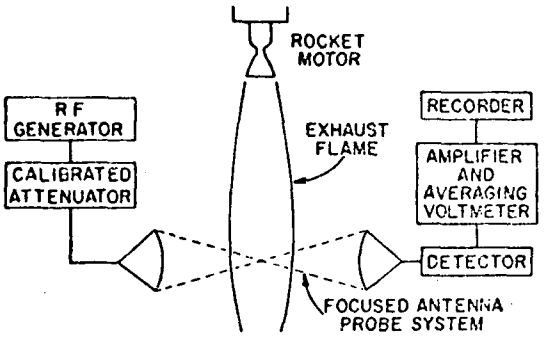

Figure 7. Apparatus for Attentuation Measurements in Rocket Exhausts (from Ref. 49).

Attenuation measurements have been used to study small laboratory test flames[50-54] as well as rocket exhausts. However, when applied to small systems, wavelength considerations severely limit the spatial resolution possible. In addition, an examination of the frequency requirements outlined above reveals that, regardless of the system under study, the attenuation method is applicable only when $n_e \gtrsim 10^{10}$ cm^{-3}. For these reasons, cavity resonance has essentially replaced attenuation in the study of laboratory scale flames.

Microwave reflection (scattering) represents an alternative method for characterizing the electrical properties of large scale combustion systems.[55,56] The apparatus[57,58] for these measurements is similar in design to those employed in attenuation determinations and the applicable range of wavelengths is identical. This technique is a difficult one to apply, however, being very sensitive to the conditions at the plasma boundaries.[59,60] In general, it is sufficiently accurate only for order of magnitude estimates of n_e at concentrations of 10^{12} cm^{-3} and higher. Measurements of electron densities via determination of the refractive index are comparably insensitive[46] and somewhat more complex in the execution. They have seen very limited use.

Mass Spectrometry

A large proportion of the most recent detailed mechanistic studies of both ionic and neutral species processes in combustion systems have been performed using mass spectrometers equipped with specially designed sampling systems. These instruments, whether applied to studies of neutrals or ions, share the advantages inherent to mass spectrometry and the problems associated with obtaining representative, chemically frozen, gas samples. A discussion of the molecular beam sampling systems used to investigate neutral species is beyond the scope of this paper and the interested reader is instead referred to some examples in the literature.[61-64] In principle, however, the experimental objectives are the same: one must withdraw a gas sample from the system and then, somehow, terminate chemical reactions and separate the species of interest from the remainder of the sample. The first of these goals is accomplished by expanding the gas through a nozzle or orifice into a vacuum. The reduction in pressure accompanying the expansion affectively freezes all but the most rapid chemistry by decreasing the molecular collision frequency; the corresponding decrease in temperature also retards all chemical reactions except those with little or no activation energy. In molecular beam work, the central portion of the expanding gas jet (comprising molecules which have not undergone collisions with the walls) is then separated from the remainder of the gas by a 'skimmer' which allows the molecules near the axis to flow into a second chamber containing the mass spectrometer and its ion source. In the sampling of ions, the function of the skimmer is performed by electrostatic lenses shown schematically[65] in Fig. 8. The whole process of ion sampling is thus simplified by two factors: the absence of gas dynamic problems associated with the skimmer and the elimination of the ion source.

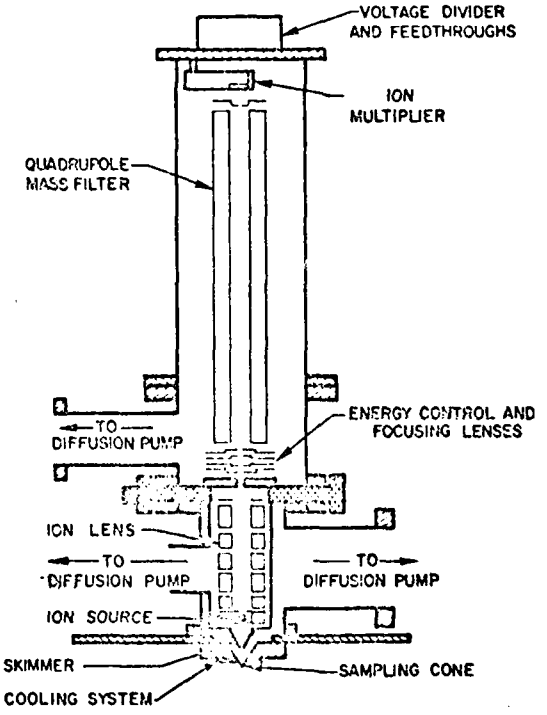

Figure 8. Flame Ion Mass Spectrometer (from Ref. 65).

The sampling orifice in typical instruments is usually placed at the tip of a cone. If condensable materials are to be present in the flame,

the cone is constructed of a material (e.g. quartz[62] or stainless steel,[63]) which will not conduct heat away rapidly thus allowing the tip to become hot and prevent condensation. The cone angle represents a compromise between being as large as possible on the inside to facilitate pumping and ion acceleration and as small as possible on the outside to minimize disturbance to the flow of flame gases. In practice, overall cone angles of about 90° are typical. The extent to which the flame chemistry is frozen is the major concern in sampling. An analysis of this problem by Hayhurst and Telford[64] using a simple gas dynamic model of the sampling process, indicates the critical available time during which unwanted chemical reactions (i.e. those which occur under conditions not representative of the combustion system, e.g. at lower temperature) can occur is of the order 10^{-7} sec. This number provides a basis for estimating whether or not significant errors of this nature are possible. For example, in the instance of an ion-molecule reaction between an ion at a concentration of 10^{10} cm^{-3} and a neutral free radical at 10^{15} cm^{-3} (both of which are typical of flames at 1 atm), significant alteration of the ion concentration during sampling will occur if the rate constant for the reaction is larger than about 10^{-8} cm^3 $molec^{-1}$ sec^{-1}. This is a large value not commonly encountered even among ion-molecule reactions.[67,68]

Once ions have been sampled and focused into a mass spectrometer, the nature of the apparatus is unimportant except that its throughput efficiency will determine the signal strength at the ion detector and the system being studied should be shielded from any strong fields associated with its operation. The pioneering research on ionization in flames was performed with magnetic[69,70] and r.f.' instruments but now, quadrupole mass filters are the most commonly employed[64, 65, 71, 72] because of their high transmission efficiency and readily controllable resolution (one is always obtained at the expense of the other). Both positive and negative ions are routinely studied in these mass spectrometers and, by matching the initial orifice size to the combustion system pressure, flames at a few Torr to 1 atm pressure can be sampled.

The instrument parameter which imposes the greatest limitations on overall mass spectrometer response is the ion transmission through the region immediately downstream of the sampling orifice. Most of the ion losses occur here through collisions with the walls of the system. Because of the non-reproducibility of these effects and the sensitivity of electrostatic focusing fields to pump oil and dirt deposits on lens components, absolute calibration of the apparatus is nearly impossible. It is feasible to use comparison of an ion current to that produced by a known concentration of, say, alkali metal ions, but even this procedure must be done carefully to account for such things as changes in mass filter throughput and multiplier response with mass. Despite these shortcomings and the unavoidable complexity of the apparatus, mass spectrometry is still the most powerful and versatile tool available for the study of combustion plasma chemistry.

ACKNOWLEDGMENT

The author wishes to express appreciation on behalf of many workers in the field of flame plasma chemistry, including himself, to the Office of Naval Research under whose sponsorship many of the techniques here described were developed and applied. Additional thanks are due the same agency for their support through Contract N00014-74-C-0326 for the preparation of this paper.

REFERENCES

1. Huddlestone,R.H. and Leonard, S.L., eds., Plasma Diagnostic Techniques, Pure and Applied Physics Series, Vol. 21 (Academic Press, New York, 1965), Chap. 5-10.
2. Gaydon, A.G., Spectroscopy of Flames (Chapman and Hall, London, 1957).
3. McWilliam, I.G. and Dewar, P.A., Nature 181, 760 (1958).
4. Dick, R. and Hartmann, H., "Critical Evaluation of the Response Characteristics of the Hydrogen Flame Detector," Varian Aerograph Tech. Bull. 133-67, 1966.
5. Hayhurst, A.N. and Telford, N.R., J.C.S. Faraday I71, 1352 (1975).
6. Sternberg, J.C., Galloway, W.S., and Jones, D.T.L., Gas Chromatography, N. Brenner, J.E. Cullen, and M.D. Weiss, eds., (Academic Press, London, 1962), p. 231.
7. Calcote, H.F., "Ion and Electron Profiles in Flames," Ninth Symposium (International) on Combustion (Academic Press, New York, 1963), p. 623.
8. Travers, B.E.L. and Williams, H., "The Use of Electrical Probes in Flame Plasmas," Tenth Symposium (International) on Combustion (The Combustion Institute, Pittsburgh, 1965), p. 657.
9. Silla, H. and Dougherty, T.J., Combust. Flame 18, 65 (1972).
10. Wortberg, G., "Ion-Concentration Measurements in a Flat Flame at Atmospheric Pressure," Tenth Symposium (International) on Combustion (The Combustion Institute, Pittsburgh, 1965), p. 651.
11. Calcote, H.F., Kurzius, S.C., and Miller, W.J., "Negative and Secondary Ion Formation in Low Pressure Flames," ibid., p. 605.
12. Jensen, D.E. and Travers, B.E.L. "Flame Plasma Diagnostic Techniques," IUPAC International Symposium on Plasma Chemistry, Kiel, Germany, September 1973.
13. Yanagi, T., Japan. J. Appl. Phys. 7, 605 (1968).
14. Yanagi, T., ibid., p. 656.
15. Bohn, D., Burhop, E.H.S., and Massey, H.S.W., The Characteristics of Electrical Discharges in Magnetic Fields, A. Gutherie and R.K. Wakerling, eds. (McGraw Hill, New York, 1949), Chap. 2.
16. Calcote, H.F., "Ion Production and Recombination in Flames," Eighth Symposium (International) on Combustion (Williams & Wilkins, Baltimore, 1962), p. 184.
17. King, I.R. and Calcote, H.F., J. Chem. Phys. 23, 2203 (1955).
18. Jensen, D.E. and Kurzius, S.C., Combust. Flame 13, 219 (1969).
19. Von Engel, A.J. and Cozens, J.R., Proc. Phys. Soc. 82, 85 (1963).
20. Ahard, M.D., International Symposium on MHD Electrical Power Generation, Eur. Nuc. Energy and Org. for Econ. Coop. and Dev. Vol. 1, p. 21, 1964.

21. Carabretta, R. and Porter, R.P., "Absolute Positive Ion Concentration Measurements in Flames with Langmuir Probes," Twelfth Symposium (International) on Combustion (The Combustion Institute, Pittsburgh, 1965), p. 605.
22. Taran, E.N. and Tverdokhlevob, V.I., Teplofiz. Vys. Temp. 4, 160 (1966).
23. Bradley, D., and Ibraham Said, M.A., J. Phys. D: Appl. Phys. 6, 465 (1973).
24. Bradley, D., Jesch, L.F., and Sheppard, C.G.W., Combust. Flame 19, 237 (1972).
25. Porter, R.P., Combust. Flame 14, 275 (1970).
26. See the discussion p. 688, ff., following Ref. 8.
27. Su, C.H. and Lam, S.H., Phys. Fluids 6, 1479 (1963).
28. Lam, S.H., AIAA J. 2, 256 (1964).
29. Johnson, E.O. and Malter, L., Phys. Rev. 80, 58 (1950).
30. Cohen, I.M., Phys. Fluids 6, 1492 (1963).
31. Swift, J.D. and Schwar, M.J.R., Electrical Probes for Plasma Diagnostics (American Elsevier, New York, 1969).
32. Jensen, D.E., "Microwave and Optical Studies of Metallic Derivatives in Flames," Ph.D. Dissertation, Cambridge Univ., 1965.
33. Padley, P.J. and Sugden, T.M., "Some Observations on the Production and Recombination of Ions and Electrons from Metallic Additives in Hydrogen and Hydrocarbon Flames," Eighth Symposium (International) on Combustion (Williams & Wilkins, Baltimore, 1962), p. 164.
34. Sugden, T.M., and Thrush, B.A., Nature 168, 703 (1951).
35. Sugden, T.M. and Wheeler, R.C., Disc. Faraday Soc. 19, 76 (1955).
36. Jensen, D.E. and Padley, P.J., "Kinetic Studies of Ionization and Recombination Processes of Metallic Additives to Flames," Eleventh Symposium (International) on Combustion (The Combustion Institute, Pittsburgh, 1967), p. 351.
37. Calcote, H.F. and Miller, W.J., "Chemical Reactions in Flame Plasma," Reactions Under Plasma Conditions, Vol. II, M. Venugopalan, ed. (John Wiley & Sons, New York, 1971), p. 327.
38. Miller, W.J., "Ions in Flames: Evaluation and Prognosis," Fourteenth Symposium (International) on Combustion (The Combustion Institute, Pittsburgh, 1973), p. 167.
39. Sugden, T.M., "Review - Elementary Combustion Reactions, Charged Species," Tenth Symposium (International) on Combustion (The Combustion Institute, Pittsburgh, 1965), p. 539.
40. Bulewicz, E.M., J. Chem. Phys. 36, 385 (1962).
41. Bulewicz, E.M. and Padley, P.J., "A Cyclotron Resonance Study of Ionization in Low Pressure Flames," Ninth Symposium (International) on Combustion (Academic Press, New York, 1963), p. 633.
42. Bulewicz, E.M. and Padley, P.J., "A Study of Ionization in Cyanogen Flames at Reduced Pressure," ibid., p. 647.
43. Bulewicz, E.M. and Padley, P.J., J. Chem. Phys. 36, 2231 (1962).
44. Bradley, J.N. and Tse, R.S., Nature 222, 474 (1969).
45. Gray, E.P., Ninth Symposium (International) on Combustion (Academic Press, New York, 1963), discussion p. 654.
46. Lawton, J. and Weinberg, F.J., Electrical Aspects of Combustion (Clarendon Press, Oxford, 1969), Chap. 5.
47. Nichol, J., Siminski, V., and Wolfhard, H.G., "Ionization in Rocket Exhausts," Eighth Symposium (International) on Combustion (Williams & Wilkins, Baltimore, 1962), p. 235.
48. Maise, G. and Sabadell, A.J., AIAA J. 8, 895 (1970).
49. Balwanz, W.W., "Ionization in Rocket Exhausts," Tenth Symposium (International) on Combustion (The Combustion Institute, Pittsburgh, 1965), p. 685.
50. Sugden, T.M., "Microwave Studies in the Ionization of Alkali Metals in Flame Gases and Related Phenomena," Fifth Symposium (International) on Combustion (Reinhold, New York, 1955), p. 406.
51. Belcher, H.E. and Sugden, T.M., Proc. Roy. Soc. A202, 17 (1950).
52. Smith, H. and Sugden, T.M., Proc. Roy. Soc. A211, 31 (1952).
53. Shuler, K.E. and Weber, J., J. Chem. Phys. 22, 491 (1954).
54. Schneider, J. and Hofmann, F.W., Phys. Rev. 116, 244 (1959).
55. Gardner, A.L., Engineering Aspects of MHD, C. Mannal and N.W. Mather, eds. (Univ. of Columbia Press, New York, 1962), p. 438.
56. Williams, H., Wilson, A.S., and Blake, C.C., Electronics Letters 7, 595 (1971).
57. Wharton, C.B. and Garner, A.L., "Microwave Circuits and Horns for Plasma Measurements," U.S. Patent 2,971,153 (1959).
58. Heald, M.A. and Wharton, C.B., Plasma Diagnostics with Microwaves (John Wiley & Sons, New York, 1965).
59. Pergament, H.S. and Siminski, V.J., "Radar Reflectivity of Turbulent Rocket Exhaust Plumes," Ninth Liquid Propulsion Symposium, CPIA Publ. No. 155, Vol. I (Applied Physics Lab., Johns Hopkins Univ., Silver Spring, 1967), p. 465.
60. Jarem, J., "Radar Reflectivity of Turbulent Rocket Exhaust Plumes - Derivation of Equations," AeroChem TP-167 Suppl., AFRPL-TR-67-251, DDC AD 863 982, November 1969.
61. Ross, J., ed. Molecular Beams (Interscience, New York, 1966).
62. Lazzara, C.P., Biordi, J.C., and Papp, J.F., Combust. Flame 21, 371 (1973).
63. Hastie, J.W., Combust. Flame 21, 187 (1973).
64. Parber, F. and Srivastava, R.C., Combust. Flame 20, 33 (1973).
65. Jensen, D.E. and Miller, W.J., J. Phys. Chem. 53, 3287 (1970).
66. Hayhurst, A.N. and Telford, N.R., Proc. Roy. Soc. A322, 483 (1971).
67. Calcote, H.F. and Jensen, D.E., "Ion Molecule Reactions in Flames," Ion-Molecule Reactions in the Gas Phase (American Chemical Society, 1966), p. 291.
68. Ferguson, E.E., Fehsenfeld, F.C., and Schmeltekopf, A.L., "Flowing Afterglow Measurements of Ion-Neutral Reactions," Adv. At. Mol. Physics, V. 5, 1, 1969.
69. Deckers, J. and Van Tiggelen, A., Nature 181, 1460 (1957).
70. Knewstubb, P.F. and Sugden, T.M., Nature 181, 474 (1957).
71. Hayhurst, A.N., Mitchell, F.R.G., and Telford, N.R., Int. J. Mass Spec. Ion Phys. 7, 177 (1971).
72. Spokes, G.N. and Evans, B.E., "Ion Sampling from Chemical Plasmas," Tenth Symposium (International) on Combustion (The Combustion Institute, Pittsburgh, 1965), p. 639.